University of Stavanger

Faculty of Science and Technology

MASTER'S THESIS

Study program/ Specialization: Marine and Offshore Technology	Autumn Semester, 2020 Open/~~Restricted~~ access
Writer: Suharmadi	(Writer's signatrue)
Faculty supervisor: Yihan Xing External supervisor: -	
Title of thesis: Preliminary Design and Optimization of Subsea Shuttle Ring-Reinforced Pressure Hull using the Response Surfaces Methodology	
Credits (ECTS): 30	
Key words: Subsea Shuttle, Parameter Correlation, Response Surface Methodology, Hydrostatic Load, Buckling, Optimization Method	Pages: 88 Stavanger, January 31, 2021

Abstract

Pipelines and tanker ships are the main hydrocarbons transportation systems operate in the North Sea. Oil and gas fields in remote and harsh locations cannot be served well by these two transportation systems. One of the main obstacles is the weather. In an effort to answer the above needs, a new hydrocarbon transportation system is developed which is expected to combine the advantages of pipeline and tanker technology while eliminating the weaknesses of both technologies. The new alternative hydrocarbon transportation system came in the form of submarine called subsea shuttle.

Subsea shuttle is designed to be able to operate at certain depths. Thus, the hydrostatic load encountered will be varied and high. This challenge requires a pressure hull design that is able to withstand the environmental loads. Otherwise, the buckling may occur. A pressure hull that is well designed, usually large and heavy. This will cause the development of the subsea shuttle to be expensive and inefficient. The optimization method can be used to maximize pressure hull performance without significantly increasing its size and weight. By determining the key parameters that affect the pressure hull, an optimum pressure hull design can be obtained.

Keyword:

Subsea shuttle, Parameter correlation, Response surface methodology, Hydrostatic Load, Buckling, Optimization method

Acknowledgement

I would like to offer my deepest gratitude to Prof. Yihan Xing for his support inside and outside the class, over his ideas, and furthermore for his understanding of my situation in many difficult times.

I also would like to thank my fellow students and faculty staffs for the collaborative environment and the supports during my study in University of Stavanger.

And lastly and obviously the biggest appreciation, to my wife Lislis and my sons Dhanis and Bagas: I love you.

Stavanger, January 2021

Suharmadi

Table of Contents

List of Figures

List of Tables

Nomenclature

ε_x	Normal strain in x-direction
ε_y	Normal strain in y-direction
γ_{xy}	Shear strain in x-y plane
R	Radius
k_x	Principal curvature to the element in x-direction
k_y	Principal curvature to the element in y-direction
σ_x	Normal stress in x-direction
σ_y	Normal stress in y-direction
M_x	Bending moment per unit length in x-direction
M_y	Bending moment per unit length in y-direction
M_{xy}	Twisting moment per unit length in x-y plane
Q_x	Transverse shear force per unit length in x-direction
Q_y	Transverse shear force per unit length in y-direction
θ	Displacement angle
χ	Twisting moment
D	Bending stiffness
E	Young's Modulus
ν	Poisson's Ratio
h	Shell thickness
λ	Load multiplier
λ_{cr}	Critical load multiplier
δ	Displacement
P	Pressure
P_{cr}	Critical Pressure
$\rho_{X,Y}$	Pearson Correlation
$\rho_{rgX,rgY}$	Spearman Correlation
ρ	Density
g	Gravitational acceleration
F	Force

R_m	Cylindrical shell mean radius
R	Internal radius of the cylindrical shell
s	Cylindrical shell nominal wall thickness
h_w	Web height of the frame
s_w	Web thickness of the frame
b_f	Flange width of the frame
s_f	Flange thickness of the frame
L_F	Frame spacing
R_C	Radius to the center of gravity of the frame cross section
R_f	Inner radius to the flange of the frame

1. Introduction and Background

1.1 Subsea transportation

In an oil and gas field development concept, hydrocarbons transportation plays an important and irreplaceable role. Oil and gas are often produced in a remote harsh environment away from the consumers; as a result, transportation networks are required to carrying the unprocessed hydrocarbons to processing facilities. The means to deliver oil and gas from the wellhead to the market requires various transportation and storage technologies. Hydrocarbon transportation methods that are often used in the development of offshore oil and gas are subsea pipeline and shipping.

Subsea pipeline is one of the most conservative methods to transport oil and gas from the offshore fields to consumers. This technique has been used since the Second World War era when the Allied Force designed the *Pipeline under the Ocean* (PLUTO). This project was intended to connect the British side to the French along the English Channel. The goal was to supply war fuel for the Allied Forces in European campaign [1]. Although PLUTO did not work as expected, this project was the first step in oil transportation by utilizing pipeline network. The first commercial subsea pipeline was built in the Gulf of Mexico on 1954 [2].

The advantages of pipeline networks as a means of hydrocarbon transportation are

- Reliable and proven technology
- No weather constraints
- Maintenance is relatively easy
- Capacity can easily be adjusted by modify its diameter or pressure

However this technology also has shortcomings including:

- Fixed location so that supply is dedicated to the single point market
- Cannot be reused after disassembly
- Relatively expensive and uneconomic for marginal fields
- Pipeline installation is often considered to damage the natural environment
- Susceptible to flow assurance problem
- Prone to leakage or damage in the event of an earthquake or other disaster.

Hydrocarbon transportation alternative which is also often used in offshore field operations is tanker ship. The first oil tanker was operated in 1863 on the river Tyne, England [3]. Furthermore, the first modern oil tanker was Zoroaster, built in early 1878 and operated in the Caspian Sea. This oil tanker was made by Ludvig and Robert Nobel [4]. Modern oil tankers operating today, comes in various types and sizes. The fluid being transported is not limited to oil, but also gas in various phases. Therefore ship tankers for gas transportation are more varied compared to oil, for example LPG tankers, CNG tankers and LNG tankers.

The benefits of tankers as a hydrocarbons transportation method are:

- Reliable and proven technology
- Supertankers are able to carry large amounts of oil. Some supertankers are able to carry up to 2 million barrels of oil at once
- Ship tankers are able to serve multiple port/market
- Not influenced by flow assurance

Meanwhile the drawbacks are:

- Highly affected by weather
- Massive supertanker cannot be docking on all ports
- Expensive manufacturing costs
- Expensive operating costs
- Not economical for remote and marginal fields
- In the event of an accident can result in an ecological disaster
- On some types of offshore platforms requires additional storage installation

Both of these hydrocarbon transportation modes are commonly used in oil and gas exploration and production activities in Norway. However, at the present time when proven oil blocks with a large production began to mature and decline, oil companies are required to explore the frontier fields which located further away and harsher environment. Additionally, the fields with small and remote reserves also start to gain more attention.

This new challenge makes both conventional hydrocarbon transportation methods unattractive. The harsh environment makes it difficult for tankers to operate on a regular basis. As a result, the shuttle tanker operation will be delayed; the field will stop production due to lack or limited storage. In the long run, it will cause loss of production opportunity and lead to reduced company revenue. Meanwhile the choice of pipeline installation is also not cost-wise, considering remote locations require a long pipeline in return of a small production.

To overcome this problem, a new transportation mode is needed and expected to accommodate the advantages of pipeline and tanker technology, while eliminating the shortcomings of both technologies. The alternative solution is called Subsea Shuttle and came in the form of an unmanned submarine which designed to be able operates in any weather, serves multiple customers/ports, and also not being restricted to one dedicated field. In the future development this submarine is also designed to work autonomously.

This thesis project suggests preliminary development of subsea shuttle which focuses on pressure hull design and optimization based on DNVGL RU NAVAL Part 4. The project will compare the characteristic of significant parameters from the calculation based on the formula given in the DNVGL RU NAVAL Part 4 using MATLAB and the simulation result from software (ANSYS). In addition, through a statistical approach this thesis will give an optimum value compared to the base parameter.

1.2 Subsea shuttle pressure hull

Submarine pressure hull configuration generally consists of ring-stiffened cylindrical shells, stiffened/unstiffened spherical shells, stiffened conical shells, and unstiffened as well as ring-stiffened prolate spheroids [5].

Burcher *et al.* [6] stated that pressure hull structures contribute a large amount to the total weight of submarines. Consequently the structure design must be as efficient as possible to reduce this weight. Reduction of structural weight for submarine can be achieved through optimization of structural dimensions, selection of lighter materials, and fit for purpose structural design.

Additionally, Burcher *et al* [6] compared the weight between a diesel-electric submarine (SSK) and a nuclear-powered general-purpose submarine (SSN), as shown in the following Table 1.

Table 1 Comparison of SSK and SSN Weight Percentage [6]

	SSK Weight (%)	SSN Weight (%)
Payload	9	8
Structure	43	45
Main and Auxiliary Machinery	35	35
Accommodation and Outfit	4	4
Stores	1	1
Permanent Ballast	8	7

The comparison of the two submarine classes above is showing that the structure dominates the weight of both of them by up to 45%.

Shape of the pressure hull

As mentioned in the previous paragraph, one of the methods to reduce subsea shuttle weight is by optimizing the structural dimension. This means that the structure must be designed optimally by maximizing the properties of the selected material. The dimensions of the structure are greatly influenced by the geometry of the subsea shuttle. The pressure differential applied to the structure is assumed to be uniform for practical application. It means the difference of pressure between top and bottom of the hull is relatively small. According to Burcher *et al* [6] there are 3 ideal shapes for pressure vessel hull geometry. The illustration for the ideal shape pressure hull is showing by Figure 1.

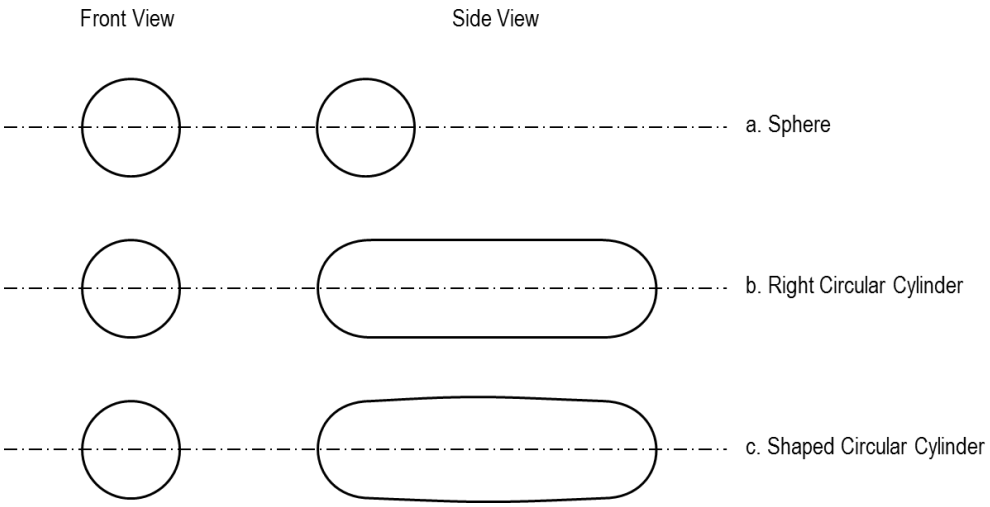

Figure 1 Pressure hull ideal shape [6]

a. Sphere

The thin sphere shell under uniform differential pressure will result in equal strains and stress all through of material of the shell. Although naturally the internal pressure is higher than external pressure, the opposite effect is happened for underwater vessel; the external pressure is higher than the internal. Therefore, this shape is ideal for uniform pressure and mostly applied for the small submarines. Nonetheless, this geometry is not suitable for the vessel which required speed for its objective. Since the hydrodynamic of this geometry will create a lot of drag force which reduces the speed substantially. Figure 2 shows the application of a sphere shell in a small submarine commonly used for recreational and observation.

Figure 2 Aurora Submarine - Courtesy to Seamagine

b. Right Circular Cylinder

The geometry of right circular cylinder with domed caps at both ends is the most efficient pressure hull structure after the sphere. This geometry is suitable to contain pressure and gives the best compatibility to fit a cylinder within streamlined form. The shape also provides many options to diverge the ratio of length and diameter. However, this geometry also is not an ideal form for hydrodynamic standpoint.

c. Shaped Circular Cylinder

This geometry is an answer to the right circular cylinder to the necessity of hydrodynamic point of view. If the design requires the pressure hulls to form the main shape of the vessel, then the geometry must follows to this outline. Streamline body can be achieved by combine cylindrical and conical section at the after-end by welding. For deep diving operated vessels the structure is considered thin in relation to its diameter, thus membrane analysis can be applied. This configuration must be more resistant to external pressure than to its internal pressure.

1.3 Thesis Objectives and Outlines

As mentioned in the sub-chapter 1.1, the objective of this thesis is to study the preliminary design and optimization of subsea shuttle ring-reinforced pressure hull geometry. This study was conducted using finite element analysis modeling, design optimization, and statistical approaches on pressure hull subjected to uniform hydrostatic pressure. ANSYS software is used in this pressure hull modeling, meanwhile, the numerical experiment based on DNVGL RU NAVAL Part 4 also carried out using MATLAB software. Further detailed objectives can be described as follows:

a. Set-up subsea shuttle pressure hull preliminary geometry and dimension.
b. Determine and investigate input parameters that influence the output parameter, including their characteristic.
c. Performs the response surfaces for the selected parameters and compares the result.

The following chart explains this thesis outline.

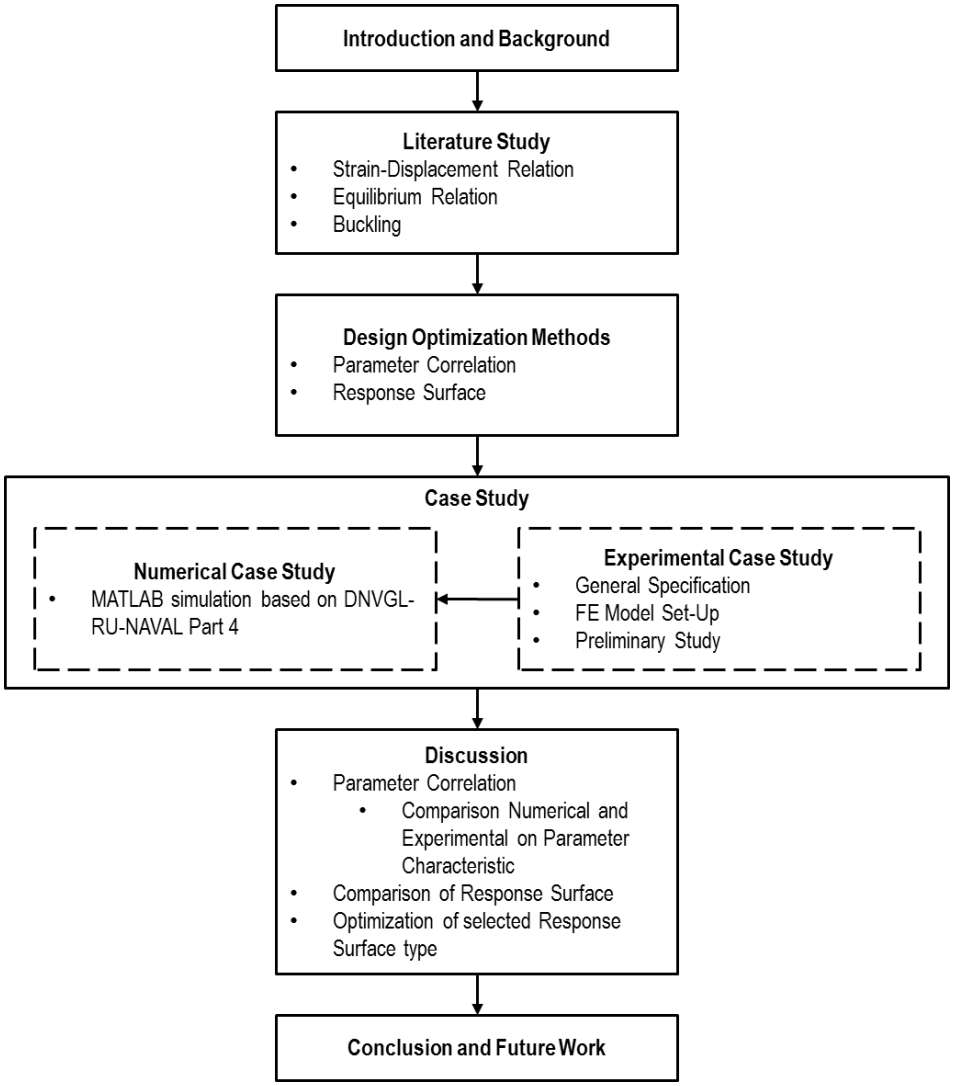

Figure 3 Thesis Outlines

Introduction and Background

This section describes the advantages and disadvantages of hydrocarbon transportation that currently exist, including the background for the development of the subsea shuttle. In addition, this part also explains the basic shape of the pressure hull that commonly used in submersibles pressure hull as the focus of this thesis. A more detailed explanation of this section is in chapter 1.

Literature Study

The scientific basis on which the pressure hull observations and experiments are based is discussed in Chapter 2. The strain-displacement relation and the equilibrium relation describe the physical reaction of the submersible pressure hull subject to external hydrostatic loads. This section also elaborates the forms and types of buckling failures that may occur on the pressure hull.

Design Optimization Methods

Chapter 3 presents the design optimization methods. There are two types of parameter correlation and five response surfaces types explained in this chapter.

Case Study

This chapter describes the subsea shuttle pressure hull experiment in which this project was configured and executed. Some preliminary studies such as mesh refinement and the effect of stiffener frame spacing are also discussed here. This experiment utilizes ANSYS software as the main tool to analyze the pressure hull subjected to external hydrostatic loads. Although not written in detail, on this occasion a numerical experiment on the pressure hull with the same dimensions and constraint was carried out using MATLAB. This calculation based on the formula given in the DNVGL-RU-NAVAL-Part 4.

Discussion

Chapter 5 presents the buckling failure modes that appear during the experiment. Then proceed with a detailed discussion related to parameter correlation and parameter determination that has a significant effect on the pressure hull configuration. The selected parameters will also be further compared with the results of numerical experiments. The results of this comparison show the characteristics of the selected parameters and are presented in the form of a scatter diagram.

The next discussion in this chapter compares the response surface results of the five types used to observe the relationship between the selected input and output parameter. The best response surface results will be further optimized.

Conclusion and Future Work

Conclusions are compiled based on the process, observation, and experimental results. Suggestions for further work are provided for the better development of a subsea shuttle.

2. Literature Study

Shell is a terminology for single or double curved body which has thickness relatively small compared to the other lateral dimension of the body [5]. Curved surfaces that divide the bounding surfaces at each middle point of thickness are called middle surface. Figure 4 illustrates a plane C intersect with middle surface plane curve P through the normal $\bar{n}$.

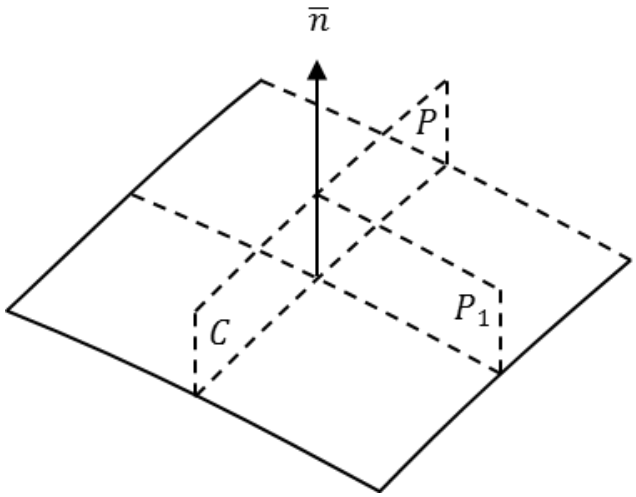

Figure 4 Middle Surface

There are infinite numbers of planes in a body which passed through normal and intersect with plane curve, similar to the Figure 4 above. For each plane curve there will be some curvature connected with it, in particular, these curvatures are unique to each other [5].

Every point on the middle surface of a shell has two curvature lines. In shell analysis, it is easier to use the curvature line of the un-deformed middle surface as the initial coordinate. Figure 5 shows point A which is at the x_1, y_1 coordinates. Generally, it is practical to use the same curvature reference lines for various strain parameters and middle surface deformation. For subsea shuttle geometry analysis, the principal direction of its basic shapes such as cylindrical, sphere, and conical can be easily determined. Due to the symmetrical shape of the subsea shuttle model, the determination of the x and z axes that coincide with the curvature will be followed by determining the starting point y axis which is coincide to normal n.

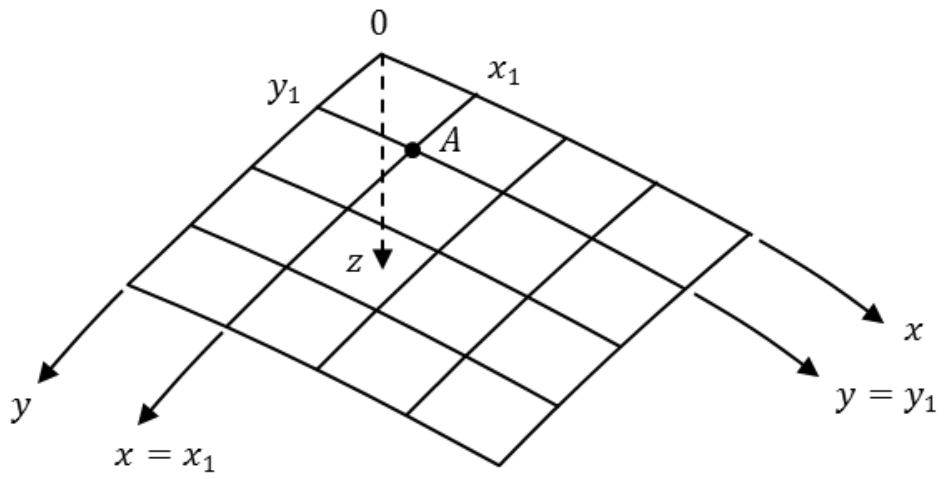

Figure 5 Curvature line on middle surface

Figure 6 illustrates the geometry of the subsea shuttle model analyzed in this thesis, which is symmetrical in the y and z directions. Hence, the analysis in both axes can be switched easily.

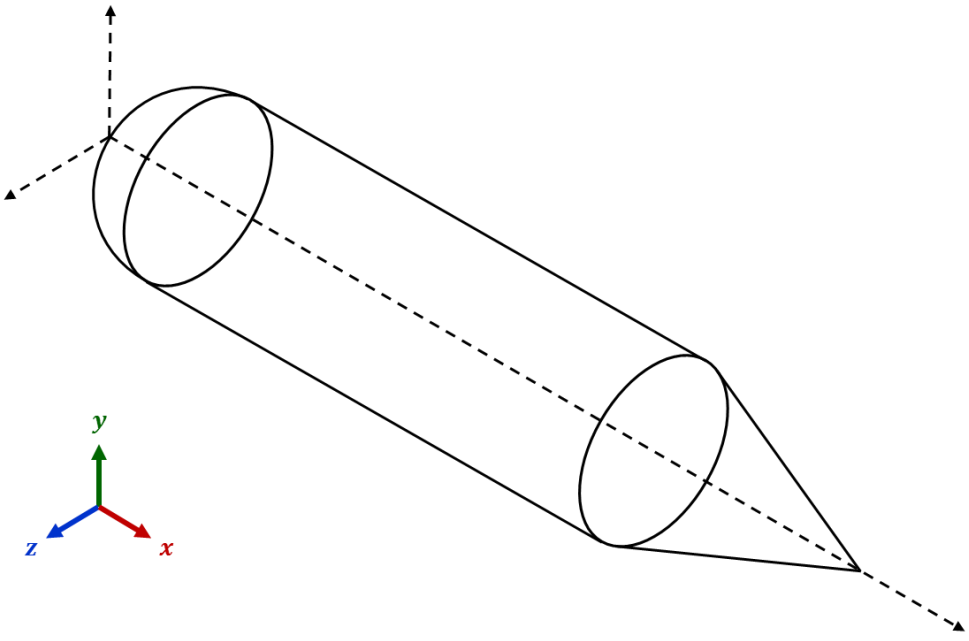

Figure 6 Subsea shuttle model direction arrangement

2.1 Strain-Displacement Relation

The projection of the extremely small middle surface element is shown in Figure 7. The element ABCD is under deformation in direction dx and dy. Henceforth, element ABCD is changing both shape and size. Due to the deformation of the middle surface, point A moves to A' by amount u and v. Meanwhile, point B displaces to B' by amount u and v with increments $\left(\frac{\partial u}{\partial x}\right) dx$ and $\left(\frac{\partial v}{\partial y}\right) dy$ respectively. Correspondingly, this displacement also applied to the point C and D. By analyzing the difference of element side length prior and after deformation, the normal strain in x and y direction can be written as:

$$\varepsilon'_x = \frac{\partial u}{\partial x} + \frac{1}{2}\left(\frac{\partial u}{\partial x}\right)^2 + \frac{1}{2}\left(\frac{\partial v}{\partial x}\right)^2 \quad \text{(Eq. 1)}$$

$$\varepsilon'_y = \frac{\partial v}{\partial y} + \frac{1}{2}\left(\frac{\partial v}{\partial y}\right)^2 + \frac{1}{2}\left(\frac{\partial u}{\partial y}\right)^2 \quad \text{(Eq. 2)}$$

These equations can be simplified further by neglecting the middle surface square derivatives, hence:

$$\varepsilon'_x = \frac{\partial u}{\partial x} \quad \text{(Eq. 3)}$$

$$\varepsilon'_y = \frac{\partial v}{\partial y} \quad \text{(Eq. 4)}$$

Applying the normal strain equations above, the middle surface shear strain γ'_{xy} due to the u and v displacements can be expressed as:

$$\gamma'_{xy} = \gamma_1 + \gamma_2 \quad \text{(Eq. 5)}$$

$$\gamma'_{xy} = \frac{\partial u}{\partial x} + \frac{\partial v}{\partial y} \quad \text{(Eq. 6)}$$

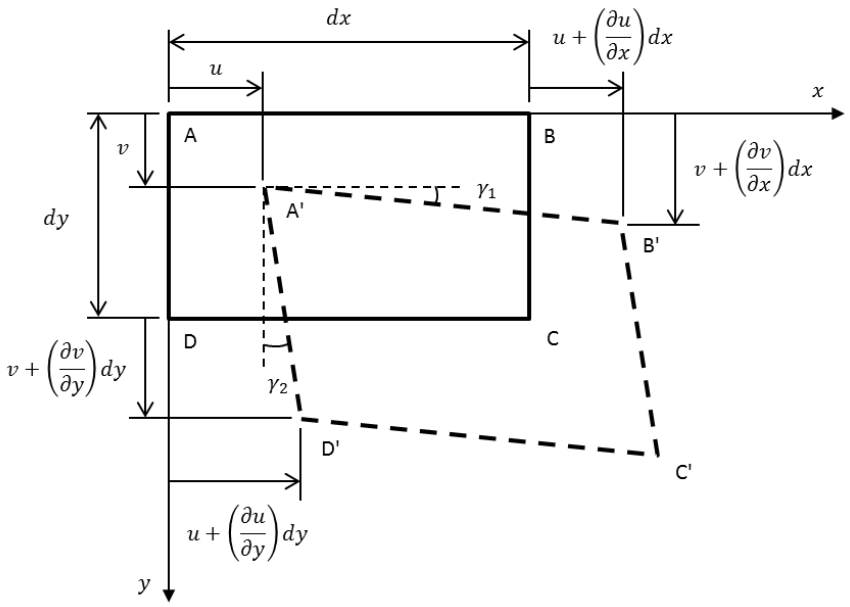

Figure 7 Infinitesmall element ABCD displace in x and y direction

If displacement w in z direction is introduced into the system (Figure 8), the equations for the normal strain in direction x and y due to the w displacement are shown in the following formula:

$$\varepsilon''_x = \frac{1}{2}\left(\frac{\partial w}{\partial x}\right)^2 \qquad \text{(Eq. 7)}$$

$$\varepsilon''_y = \frac{1}{2}\left(\frac{\partial w}{\partial y}\right)^2 \qquad \text{(Eq. 8)}$$

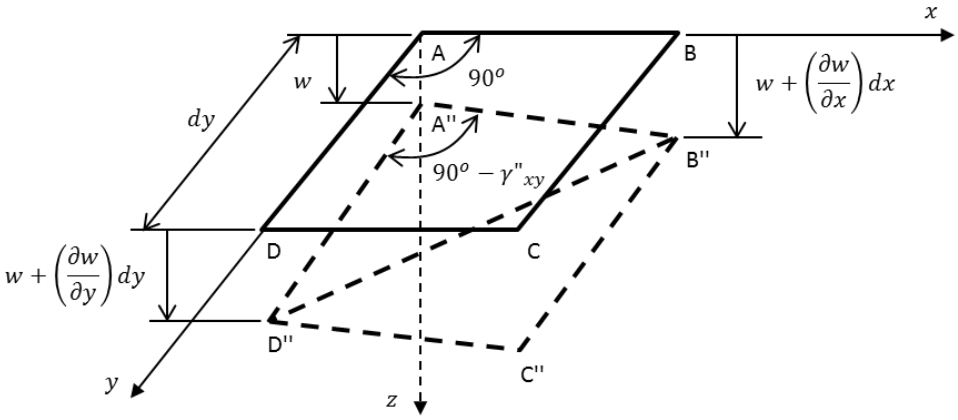

Figure 8 Infinitesmall element ABCD displace in z direction

The middle surface shear strain due to w displacement, symbolized by γ''_{xy} can be determined using law of cosines to triangle A''B''D''. Since the element ABCD is extremely small, γ''_{xy} angle is also very small, it can be neglected. Therefore, the shear strain resulted in:

$$\gamma''_{xy} = \frac{\partial w}{\partial x} * \frac{\partial w}{\partial y} \quad \text{(Eq. 9)}$$

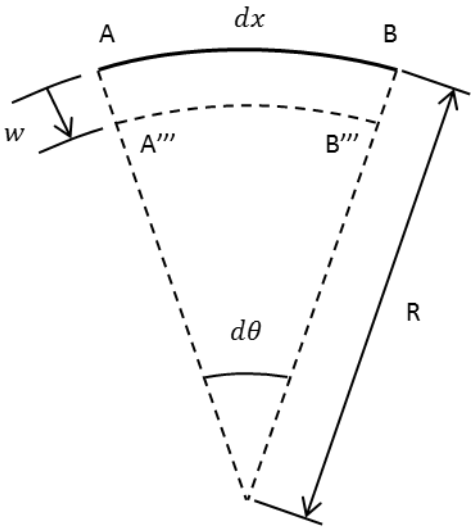

Figure 9 Element AB with w displacement

Further analysis is by situating the element to w displacement in the z-direction. In this case the effects of change of curvature are taken into consideration. The un-deformed element is marked by AB, while after deformation element is marked by A'''B'''. See Figure 9. The radius of curvature R is constant. The corresponding principal curvature to element is denoted by k_x where

$$R = \frac{1}{k_x} \quad \text{(Eq. 10)}$$

Hence, the normal strain in x and y direction is resulted in:

$$\varepsilon'''_x = -\frac{w}{R} = -wk_x \quad \text{(Eq. 11)}$$

$$\varepsilon'''_y = -\frac{w}{R} = -wk_y \quad \text{(Eq. 12)}$$

By combining the all contributing normal and shear stress, the middle surface strain-displacement relations can be written as:

$$\varepsilon_x = \frac{\partial u}{\partial x} + \frac{1}{2}\left(\frac{\partial w}{\partial x}\right)^2 - wk_x \quad \text{(Eq. 13)}$$

$$\varepsilon_y = \frac{\partial u}{\partial y} + \frac{1}{2}\left(\frac{\partial w}{\partial y}\right)^2 - wk_y \quad \text{(Eq. 14)}$$

$$\tau_{xy} = \frac{\partial v}{\partial x} + \frac{\partial u}{\partial y} + \frac{\partial w}{\partial x} * \frac{\partial w}{\partial y} \quad \text{(Eq. 15)}$$

After differentiating Eq. 13, Eq. 14, and Eq. 15 with respect to y and x accordingly, the *equation of compatibility* can be expressed as:

$$\frac{\partial^2 \varepsilon_x}{\partial y^2} + \frac{\partial^2 \varepsilon_y}{\partial x^2} - \frac{\partial^2 \gamma_{xy}}{\partial x \partial y} = \left(\frac{\partial^2 w}{\partial x \partial y}\right)^2 - \frac{\partial^2 w}{\partial x^2} * - \frac{\partial^2 w}{\partial y^2} - k_x \frac{\partial^2 w}{\partial y^2} - k_y \frac{\partial^2 w}{\partial x^2} \quad \text{(Eq. 16)}$$

2.2 Equilibrium Relations

Element ABCD is exposed to the normal and shear forces acting in the shell middle surface, shown by Figure 10. These forces are characterized by normal stress σ_x and σ_x and the shear stress τ_{xy}. Throughout the thickness h of the shell, these forces are constant and eventually lead to forces. This phenomenon is called as *membrane effect* [5]. In relation to the previous discussion, the forces acting on the face AB and AD are different than the forces on the face BC and CD due to the displacement. Similar treatment also applied for the shear stress.

By calculating the forces performed on the element ABCD, the equilibrium in x and y direction can be written as follows:

$$\frac{\partial \sigma_x}{\partial x} + \frac{\partial \tau_{xy}}{\partial y} = 0 \quad \text{(Eq. 17)}$$

$$\frac{\partial \sigma_y}{\partial y} + \frac{\partial \tau_{xy}}{\partial x} = 0 \quad \text{(Eq. 18)}$$

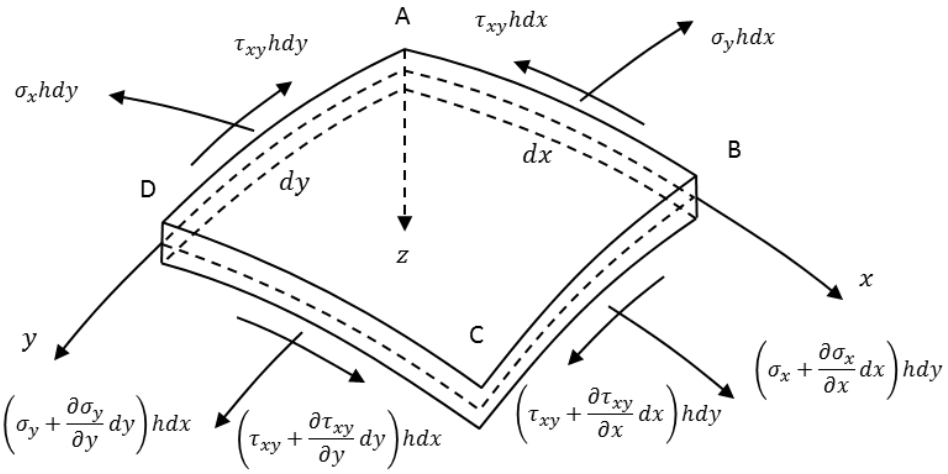

Figure 10 Elemen ABCD with Stress and Strain

If bending moment per unit length M_x and M_y, the twisting moment per unit length M_{xy}, and transverse shear forces per unit length Q_x and Q_y are applied to the element, the moment equilibrium in the x-axis resulted:

$$\frac{\partial M_y}{\partial y} + \frac{\partial M_{xy}}{\partial x} - Q_y = 0 \qquad \text{(Eq. 19)}$$

And in the y-axis as:

$$\frac{\partial M_x}{\partial x} + \frac{\partial M_{xy}}{\partial y} - Q_x = 0 \qquad \text{(Eq. 20)}$$

For thin shells application the transverse shear forces are assumed equal to zero due to the plane stress condition. Next step is to incorporated forces in the z-direction. The displacement in angle θ can be expressed as:

$$d\theta = \frac{dx}{R} = k_x dx \qquad \text{(Eq. 21)}$$

By observing the difference of change of slope due to the w displacement, the net of change of slope relative to x and y axes can be expressed as follows:

$$\left(k_x + \frac{\partial^2 w}{\partial x^2}\right) dx \qquad \text{(Eq. 22)}$$

$$\left(k_y + \frac{\partial^2 w}{\partial y^2}\right) dy \qquad \text{(Eq. 23)}$$

Where, $\frac{\partial^2 w}{\partial x^2}$ and $\frac{\partial^2 w}{\partial y^2}$ can be defined as change of curvature per unit length in the x and y direction respectively. The second derivatives of change of curvature expressions are related to bending of the shell. However, the mixed second derivatives symbolized by χ are related to twisting of the shell and expressed by this relation:

$$\chi = -\frac{\partial^2 w}{\partial x \partial y} \qquad \text{(Eq. 24)}$$

The membrane effect corresponds to the expansion and compression of shell middle surface along with the shearing acting on it. Based on the discussion above, the membrane effect is subject to bending and twisting effects which represented by M_x, M_y, and M_{xy}. This manner of shell due to membrane effect and bending effect is comparable to the beam-column theory. Hence the normal stresses, shear strain, bending moment per unit length and twisting moment per unit length can be re-written as:

$$\sigma_x = \frac{Ez}{(1-\nu^2)}\left(\frac{\partial^2 w}{\partial x^2} + \nu \frac{\partial^2 w}{\partial y^2}\right) \qquad \text{(Eq. 25)}$$

$$\sigma_y = \frac{Ez}{(1-\nu^2)}\left(\frac{\partial^2 w}{\partial y^2} + \nu \frac{\partial^2 w}{\partial x^2}\right) \qquad \text{(Eq. 26)}$$

$$\tau_{xy} = \frac{Ez}{(1-\nu)} * \frac{\partial^2 w}{\partial x \partial y} \qquad \text{(Eq. 27)}$$

$$M_x = -D\left(\frac{\partial^2 w}{\partial x^2} + \nu \frac{\partial^2 w}{\partial y^2}\right) \qquad \text{(Eq. 28)}$$

$$M_y = -D\left(\frac{\partial^2 w}{\partial y^2} + \nu \frac{\partial^2 w}{\partial x^2}\right) \qquad \text{(Eq. 29)}$$

$$M_{xy} = -D(1-\nu)\frac{\partial^2 w}{\partial x \partial y} \qquad \text{(Eq. 30)}$$

Where D is represent the flexural rigidity or bending stiffness of the shell and equal to EI of simple beam theory. While, E is Young's Modulus and ν is Poisson's Ratio. The value of D represents by the following equation:

$$D = \frac{Eh^3}{12(1-\nu^2)} \quad \text{(Eq. 31)}$$

2.3 Buckling

2.3.1 Buckling of Thin Shell

The buckling analysis for thin elastic shell analysis can be explained by the relation between load acting on it and the displacement. Since the displacement is comparably small to the size of the body, then the analysis can be done by observing the behavior of beam theory. Figure 11 is showing the comparison of column and plate. Section OA is representing the equilibrium state with no bending effect. While, section CAD represents the bent, under a moment equilibrium configuration. For the column, section CAD reached neutral equilibrium which discernible by horizontal line form. Meanwhile, for the plate the symmetrical form is showing after critical stable state relative to the ordinate axis.

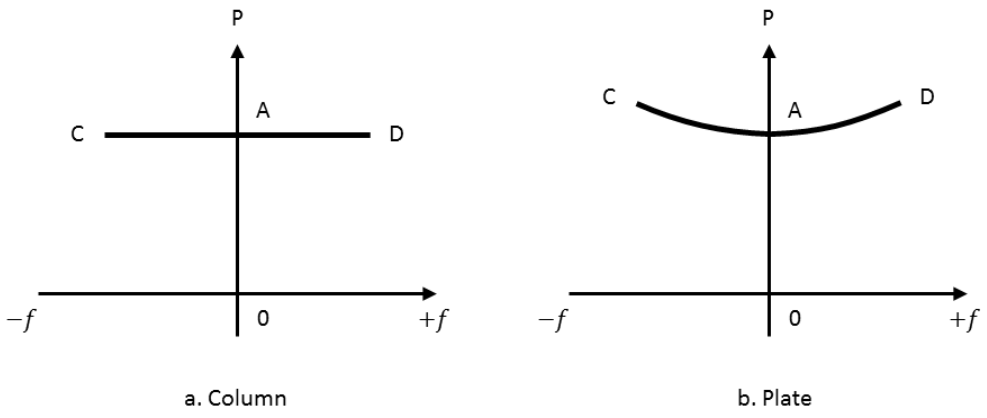

Figure 11 Column and Plate subjected to load

The thin shell is able to absorb strain energy without undergoing significant deformation. This feature is highly utilized by submerged vehicle hull design. The reason behind this behavior is the shell membrane stiffness extent several order higher than bending stiffness [9] [14]. Nonetheless, when large portion of strain energy in the form of compression stored within shell converts into strain energy of bending, the

shell possibly will buckle. This conversion only happened when the major deformation occur to the shell [8] [9].

The length/radius ratios signify the most significant aspect of compressed shell behavior. However, this aspect is having a tendency to yield in lower collapse load compared to the predicted theoretical load by linearized theory [5][15]. This occurrence is happen due to the sensitivity of the shell to the geometry imperfection e.g. cylindrical, conical, and spherical.

Bushnell [9] stated there are two types of buckling. The first type of failure is nonlinear collapse. This type of failure utilizes non-linear stress analysis to predict buckling. As the load increased, the rigidity of structure decreases. As the load increases, the stiffness of the structure decreases. The same can be seen in the slope of the load-deflection curve which decreases until it reaches neutral equilibrium. At the point of collapse, the slope of the equilibrium curvature is equal to zero and if the magnitude of acting load is remain the same during the deformation, failure happens instantaneously. This incident is often called *snap-through* [9]. The second type of failure is bifurcation buckling. This type of buckling utilized eigenvalue analysis to predict the failure. At the bifurcation point, shell deformation start to develop into a new pattern which dissimilar from the initial pattern. If the post-bifurcation equilibrium curve has negative slope and the acting load is independent, the shell failure can happen.

Figure 12 is showing the most common circumstance for the load-displacement relationship. Where, λ_L is collapse load of the perfect shell, λ_C is collapse load at bifurcation point, and λ_S is collapse load at snap-through point. The curve OAC is the fundamental axisymmetric deformation, while BD refers to non-axisymmetric deformation. The failure is begin at the point B and can be identified by rapidly growing deformation. In the actual situation where imperfection is part of the structure, the bifurcation buckling never happened. Structure material behavior will succeed the OEF curve and the failure is marked at the snap-through point E. This point is corresponding to non-symmetric displacement variable. Although, true bifurcation buckling never happened in real life event, this analysis is useful to approximate the failure load and mode [9].

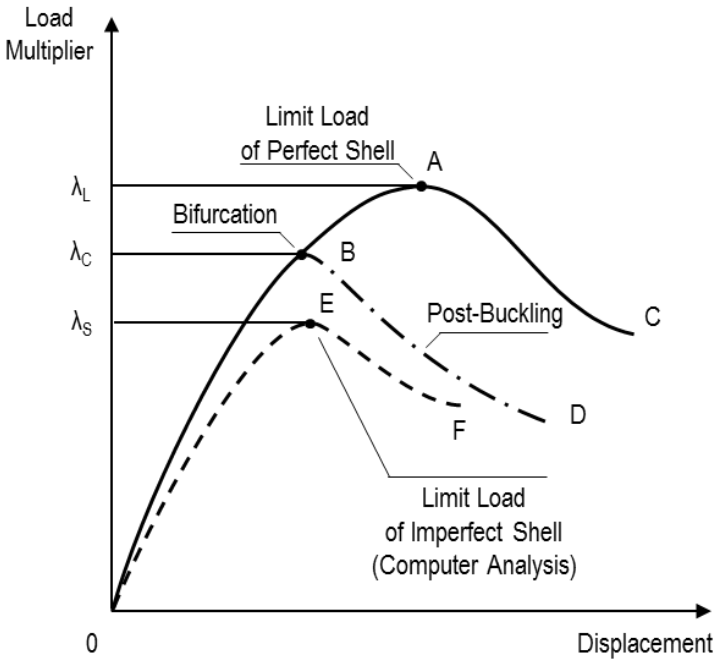

Figure 12 Total Displacement corresponds to Load Multiplier [9]

2.3.2 Eigenvalue Buckling Analysis

The eigenvalue buckling analysis is powerful to analyze the critical load of a geometrically linear structure subject to axial compression, bending, lateral pressure, etc. [7]. In this analysis the structure is assumed free from the imperfection. Stress analysis is performed on the structure introduced to the reference external random load $\{P\}_{ref}$. The stress stiffness matrix corresponding to the reference load is $[D]_{ref}$, with a scalar load multiplier λ [8].

$$[D] = \lambda[D]_{ref} \text{ when } [P] = \lambda[P]_{ref} \quad \text{(Eq. 32)}$$

The load multiplier λ multiplication in $\{P\}$ leads to in multiplication the stress intensity by λ, however, it does not influenced the stresses distribution. From the assumption, it can be stated that the conventional stiffness matrix $[D]$ is unaffected by the load. If the critical load multiplier λ_{cr} which corresponding to displacement $\{\delta\}$ is taken into consideration, the Eq X can be written as follows:

$$\left([D] + \lambda_{cr}[D]_{ref}\right)\{D_{ref}\} = \lambda_{cr}[P]_{ref} \quad \text{(Eq. 33)}$$

$$\left([D] + \lambda_{cr}[D]_{ref}\right)\{D_{ref} + \delta\} = \lambda_{cr}[P]_{ref} \quad \text{(Eq. 34)}$$

The subtraction from the both equation, resulted:

$$\left([D] + \lambda_{cr}[D]_{ref}\right)\{\delta\} = 0 \quad \text{(Eq. 35)}$$

At the point of bifurcation, the smallest load multiplier λ_{cr} represents the smallest external load $[P]_{cr}$ which may cause failure, therefore:

$$[P]_{cr} = \lambda_{cr}[P]_{ref} \quad \text{(Eq. 36)}$$

DNV RP-C208 *Determination of Structural Capacity by Non-linear FE analysis Methods* proposed three different methods to analyze buckling [16]:

a) Linearized approach by utilizing the finite element method for assessing the buckling eigenvalues (linear bifurcation analysis)
b) Full non-linear analysis using code defined equivalent tolerance and/or residual stresses
c) Non-linear analysis that is calibrated against code formulation and test.

This thesis project will use the first approach to analyze eigenvalues of the bifurcation buckling of subsea shuttle pressure hull.

2.3.3 Buckling Mode

The analysis of basic geometry without imperfection and preload stress due to effect assumption give advantages to predict critical load of the structure. However, the additional geometry circular ring-stiffener with weld-bounded increased the complexity of the stress and strain experienced by the pressure hull material [5][6].

Buckling mode on ring-reinforced cylindrical.

Nash [5] stated for the ring-reinforced cylindrical shell under hydrostatic load, the failure may presence in several modes.

a. Inelastic axisymmetric shell instability between adjoining frames. This buckling also known as inter-frame shell yielding [6]. When circumferential strain between stiffeners increased, there will be a combination between of axial loading and axisymmetric buckling. As a result additional bending strain is occurred and the cylinder may fail. This occurrence often refers as concertina mode. Figure 13 a. illustrates the partial concertina mode where the body is under external load and trying to release the pressure before failure. A V-shaped ring spanning entirely or partly around the circumference of the shell characterizes this phenomenon [5].

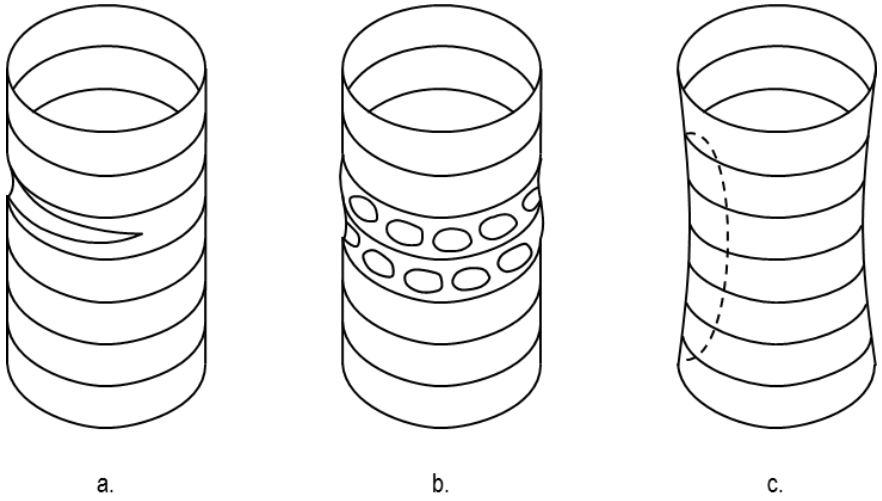

Figure 13 Failure Modes of ring stiffened thin circular cylinder [6]

b. Asymmetric collapse of the shell between adjacent frames. This failure type also known as lobar buckling. The indentations rarely extend fully around the shell circumference (localized). The failure magnitude is affected by the shape and dimension of ring-reinforced stiffeners which corresponds to asymmetric shell instability. If the bending stiffness of ring-reinforced stiffeners able to withstand to critical load, the unsupported shell will buckle [18]. Figure 13 b. illustrate this buckling mode.

c. General instability of shell and rings. Cylindrical ring-reinforced shell under external load may buckle if the supported rings are considered *weak* or *light* in comparison to the shell [5]. If the ring cross-sectional and/or inertia comparably insufficient to the shell dimension, the shell deformation will ignore the stiffeners during buckling. This failure also known as global or overall buckling. The failure mode is shown by Figure 13 c.

Buckling mode on spherical.

Spherical shell subjected to external hydrostatic load; pose to buckling problem elastically, plastically, or in the elastic-plastic region [5][6]. The experiment by Carlson *et al* [19], describes that spherical shell buckling started as a single dimple axisymmetric with a diameter of the sphere, whose size influenced by the geometry of the shell, and which form a comparatively small solid angle as shown in Figure 14. As the external load increases, the dimple deepens.

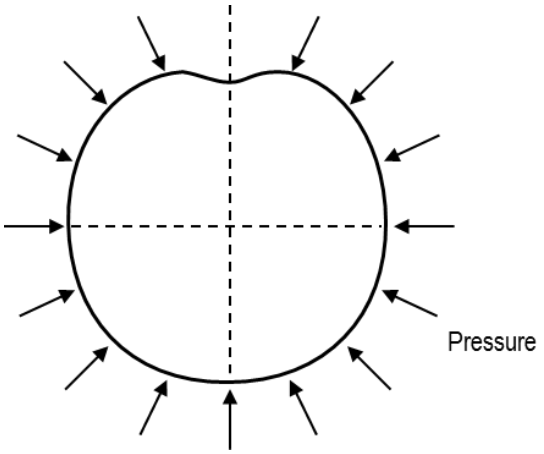

Figure 14 Cross-section of Sphere Buckling [5]

Design of modern deep submerged vehicles utilized either domes or caps of spherical shells subject to hydrostatic loading [6]. As discussed, the geometric imperfection has a major influence on the buckling of the spherical shell. If the small area of the shells has incorrectly curvature, this may fail quickly, leading to the overall collapse of the spherical shell (Figure 15 b.)

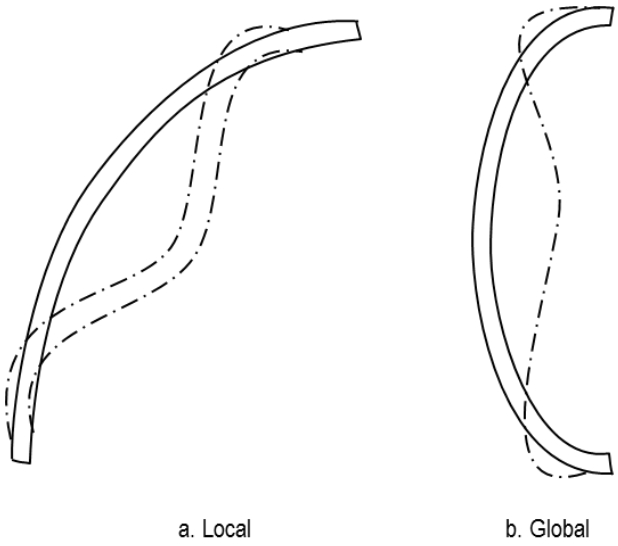

Figure 15 Dome Buckling [6]

Buckling mode on conical.

Similar to a cylindrical shell and spherical shell, the full or truncated conical shells exposed to the external load may also experience deformation and buckling elastic, plastic, or elastic-plastic. The conical shell buckling may not occur over the entire circumference. These occurrences likely were initiated by geometric imperfections in the shell that may happen before exposure to the external load, thickness deviation during fabrication, and the presence of vibrations during testing [5]. Figure 16 illustrate the buckling that may occur on conical shell.

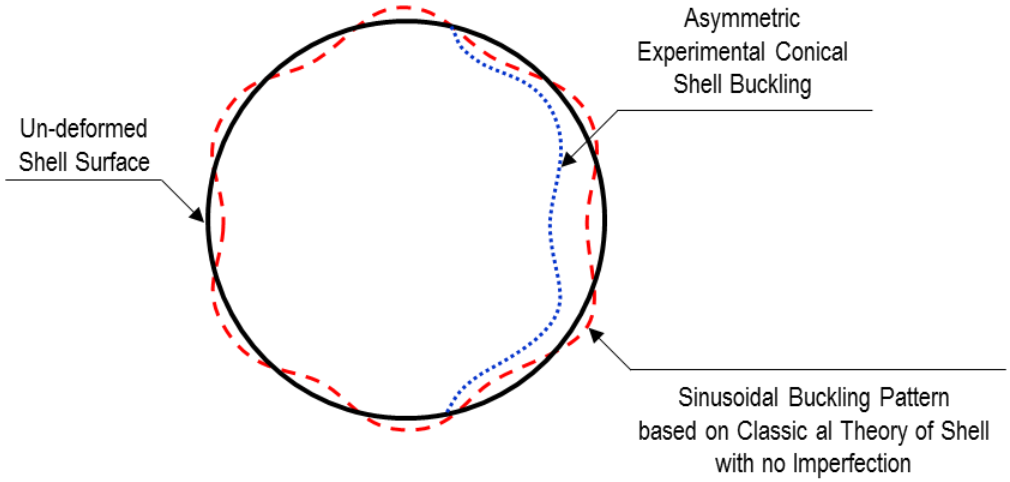

Figure 16 Cross-section of Conical Buckling [5]

Frame buckling and tripping.

To avoid unnecessary buckling, the ring stiffeners have been added to cylindrical shell. However, the ring stiffeners under an excessive load are not buckling free. The stiffeners will buckle first when the dimension of the stiffeners is not adequate to sustain the cylindrical shell [20]. A stiffener may buckle out of the cross-sectional plane or in torsional mode in connection with part of the shell plate [6]. The failure happened in the frame and stiffeners illustrates in Figure 17.

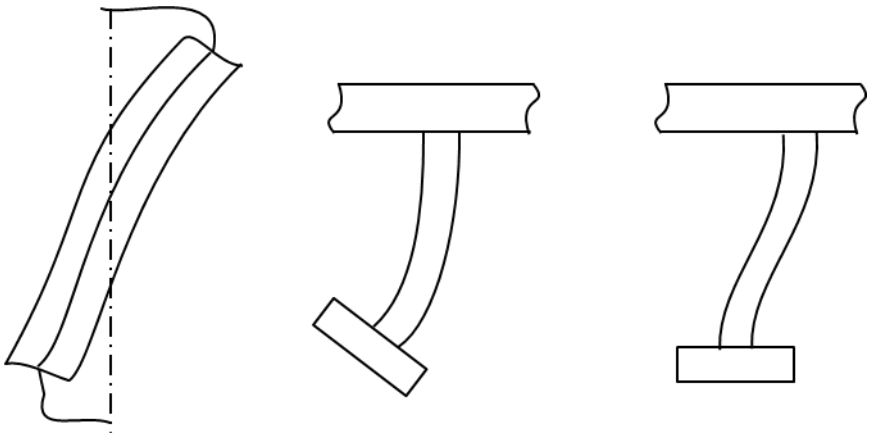

Figure 17 Frame Buckling and Tripping [6]

2.4 Failure Criteria

Buckling or the instantaneous deformation associated with the instability of the equilibrium of strain-displacement relation. This failure is often resulting in total collapse of the structure. The elastic buckling of the shell may occur when the external load reaches critical load [21].

The DNVGL-NAVAL-RU Part 4 [17] governs the collapse diving pressure (CDP) for the pressure hull. At the CDP point, the acting load leading to failure may lie in the elastic or elastic-plastic range of the material properties. The following failure types must be demonstrated that the pressures for failure are greater or equal to the collapse diving pressure [17].

- Symmetric and asymmetric buckling between the stiffeners
- General instability under consideration of the partial effect of the web frame
- Tilting of the frames
- Buckling of the dish end and spherical shell
- Local yielding in the area of discontinuities

This code provides the design safety factor equal to 1 for the collapse diving pressure.

3. Design Optimization Methods

3.1 Parameter Correlation

The relation between two or more variables from a statistical point of view can be referred as correlation. This statistical approach is useful to comprehend the interaction between variables in an experiment. The methods used to assess a correlation can generate a coefficient that represents the interaction between variables. A correlation coefficient might have positive, negative, or neutral value. A correlation with positive coefficient means that the interaction between the two variables moves in the same trend. As the first variable increases, the second variable also increases. And for the opposite, a negative coefficient means that the relationship between these two variables is inversely proportional. When the first variable has increased, the value of the second variable will decrease. Lastly, a neutral correlation coefficient means there is no interaction between the selected variables.

The magnitude of the correlation coefficient indicated in value ranged between -1 to $+1$. A coefficient value closer to -1 or $+1$ signify a strong correlation between variables, while coefficient value 0 indicates neutral correlation. Hinkle [11] wrote the interpretation of the correlation coefficients as shows in the following table:

Table 2 Correlation Coefficient Interpretation [11]

Correlation Coefficient	Interpretation
0.90 to 1.00 (−0.90 to −1.00)	Very high positive (negative) correlation
0.70 to 0.90 (−0.70 to −0.90)	High positive (negative) correlation
0.50 to 0.70 (−0.50 to −0.70)	Moderate positive (negative) correlation
0.30 to 0.50 (−0.30 to −0.50)	Low positive (negative) correlation
0.00 to 0.30 (0.00 to −0.30)	Negligible correlation

3.1.1 Pearson Correlation

The Pearson correlation method measures the strength of the linear relations between two variables. The Pearson correlation can be written as follows:

$$\rho_{X,Y} = \frac{\mathrm{cov}(X, Y)}{\sigma_X \sigma_Y} \quad \text{(Eq. 37)}$$

Where $\mathrm{cov}(X, Y)$ is the covariance, σ is the standard deviation. By evaluating a matrix for each pair of variables in the dataset, the Pearson correlation can be used to determine the correlation between more than two variables.

3.1.2 Spearman Correlation

The Spearman correlation measures interaction between two variables in nonlinear manner. In this case, the relation between variables is defined by a strong or weak rank [22]. The Spearman correlation between the two variables is proportional to the Pearson coefficient between the ranks of the two variables.

$$\rho_{rgX,rgY} = \frac{cov(rg_X, rg_Y)}{\sigma_{rg_X} \sigma_{rg_Y}} \quad \text{(Eq. 38)}$$

The relationship between the variables is assumed monotonic without linear relation. Similar to the Pearson correlation, the Spearman correlation matrix can be determined on a pair basis for each variable.

3.2 Response Surface Methodology

The preliminary subsea shuttle design discussed in this project involves many variables. To learn the response of one or more variables, it is necessary to plan and design the experiment and analyze the obtained results. The Response Surface Methodology (RSM) is a powerful method to optimize output variables. This method is introduced in the early 1950 by Box and Wilson [13]. The aim of RSM is to find the optimal response of a carefully designed experiment by taking into account all potential limitations.

In the real situation of engineering design, achieving an efficient parameter or the desired output is a prolonged process, requires massive data, and prone to error. It is understandable since the function governs the relation between input and output parameter is complex or unidentified. The RSM is useful to reduce the costly experiment by providing the approximate value close to the real measured value.

Design of Experiment (DoE) is an important aspect of the RSM. The goal of DoE is to determine the points where the response should be estimated. The RSM performs on a series of generated DoE and produced a response surface as an approximate function to estimate the relation between input and output parameter. The relation can be described as:

$$\mathrm{Output}_1, \mathrm{Output}_2, \ldots\ldots, \mathrm{Output}_n = \beta(\mathrm{Input}_1, \mathrm{Input}_2, \ldots\ldots, \mathrm{Input}_n) \quad \text{(Eq. 39)}$$

$$\mathrm{y} = \beta(x_1, \mathrm{x}_2, \ldots\ldots, \mathrm{x}_n) + \varepsilon \quad \text{(Eq. 40)}$$

Where the β is the performance function or *response surface*, y is the performance characteristic or *response*, x_i is independent variables of the number n or *explanatory*, and ε is the error or noise.

The size of generated sample data (DoE) has a great influence on the approximate value produced by the RSM. The larger data sample is considered will decrease the error between approximate and real measured value. Other factors that might affect the RSM result are the variation of the solution and the response surface type [23].

Prior to the RSM process, a screening study to filter out the irrelevant parameters is carried out. This early process is necessary to ensure that the parameters that will be input in the DoE are parameters that have a significant effect on further experiment.

This thesis will compare the influence of the five response surface types on the subsea shuttle parameters. The five of them are:

- Genetic Aggregation
- Full 2nd Order Polynomial
- Kriging
- Non-Parametric Regression
- Neural Network.

3.2.1 Genetic Aggregation

Genetic Aggregation response surface is the most effective response surface type. This method combines several different response surface types. Its algorithm allows this method to automatically select and configure the most suitable response surface type for each output parameter, and solved it simultaneously. Consequently, these features make the genetic aggregation response surface to require a longer time to complete compared to the other types. In the ANSYS, the default setting for the response surface type selection is genetic aggregation.

3.2.2 Full 2nd Order Polynomial

The RSM equation is the 1st order of polynomial form. This equation can be easily solved using a simple factorial design. This is an effective method to define the relation between explanatory variable and response variable. The 1st order polynomial equation from Eq. 40 can be rewritten as

$$y = \beta_0 + \beta_1 x_1 + \beta_2 x_2 + \varepsilon \quad \text{(Eq. 41)}$$

When the experimental design contains the optimal response point among the factor levels under investigation, the 1st order polynomial equation will contain a *lack-of-fit* [27]. Hence, the 2nd order polynomial is required. The study of the full 2nd order polynomial considers the application of the full quadratic polynomial model. The 2nd order polynomial has the equation as follows:

$$y = \beta_0 + \beta_1 x_1 + \beta_2 x_2 + \beta_{11} x_1^2 + \beta_{22} x_2^2 + \beta_{12} x_1 x_2 + \varepsilon \quad \text{(Eq. 42)}$$

3.2.3 Kriging

Kriging is response surface type which makes the most of interpolation for estimation of the best linear unbiased prediction of the intermediate values. This method uses the approach that the analyzed data is considered as the realization of random variables which as a whole form a random function that defines the relationship between variables. Kriging is also used to minimize the variance of the prediction result.

$$\hat{Z}(s_0) - m(s_0) = \sum_{i=1}^{n} \lambda_i [Z(s_i) - m(s_i)] \quad \text{(Eq. 43)}$$

Where: $\hat{Z}(s_0)$ is the measured value

$\hat{Z}(s_i)$ is the measured value at the ith location

$m(s_0)$ is the expected value of $\hat{Z}(s_0)$

$m(s_i)$ is the expected value of $\hat{Z}(s_i)$

λ is the weight factor of the measured value at the ith location$\mathrm{m}(\mathrm{s_i})$

s_0 is the predicted location

s_i is the predicted location at the ith location

n is the number of measured value

In ANSYS, Kriging is completed with auto refinement tool that iteratively update the refinement point to obtain certain desired result. In general, Kriging response surface is a reliable method to obtain estimated value.

3.2.4 Non-Parametric Regression

Non-parametric regression is response surface based on regression analysis which do not depend on predetermine model or data distribution. Typically, a data set with finite assumption parameter and distribution can be estimated with parametric regression. However, when the unknown data set with unknown distribution is given, non-parametric regression will come in handy. The result of this method is purely based on the given raw data. Consequently, to achieve the anticipated result, a larger sample is required compared to the normal parametric regression requirement.

The non-parametric regression response surface method is suitable for high nonlinear behavior response result which requires accuracy improvement. Nonetheless, where the low order polynomial data sets lead the case, the presence of oscillations may reduce the accuracy.

3.2.5 Neural Network.

The Neural Network response surface algorithm imitates the human working brain. This method approach is based on biological neural network which depends on the input. The function that will process these inputs is hidden functions that contains, collects, and classifies inputs and transmit the appropriate responses. This task is similar to the function of the human brain neuron cells which designed to transmit information to other nerve cells, muscles, or gland cells. Figure 18 shows a complete neural network configuration with interconnections arrows between inputs, hidden functions, and the outputs. The arrows connecting each of these sections represent weight of the input. The equation used in Neural Network response surface can be written as follows:

$$f_k(x_i) = K(\sum w_{jk} g_j(x_i)) \qquad \text{(Eq. 44)}$$

Where: x_i is the input parameter

g_j is the hidden function

K is the predefined function

w is the input weight factor

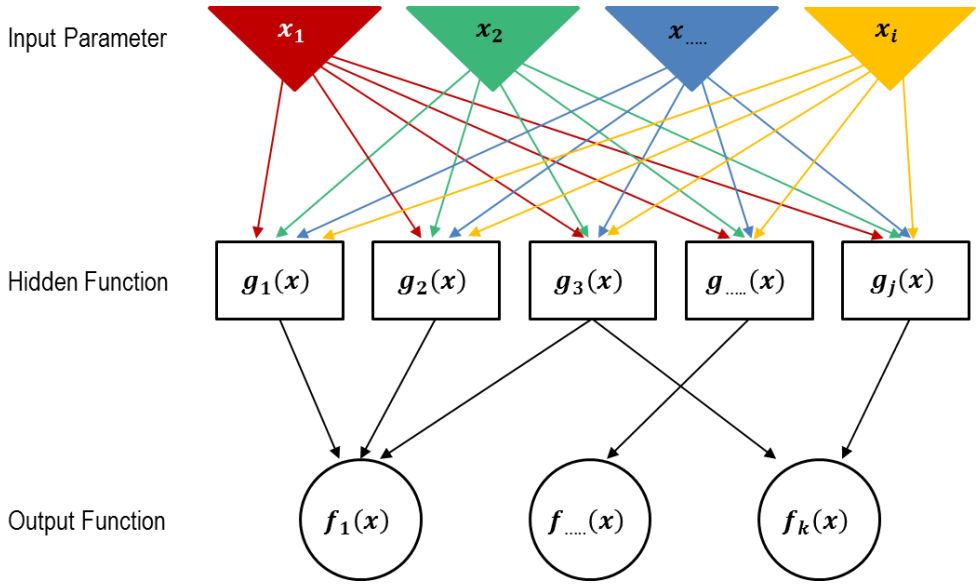

Figure 18 Neural Network Configuration

4. Case Study

4.1 Software Applications

4.1.1 ANSYS

The modeling used in this simulation uses a finite element analysis approach. In order to configure the subsea shuttle geometry and to analyze the experimental results, it is necessary to use software that is able to model the geometry and boundary conditions as closely as possible to the actual conditions. This thesis project uses ANSYS Workbench 2020 as a tool to model and analyzes the subsea shuttle pressure hull subjected to external hydrostatic loads. A flow chart showing how this experiment was done using ANSYS Workbench is shown in Figure 19.

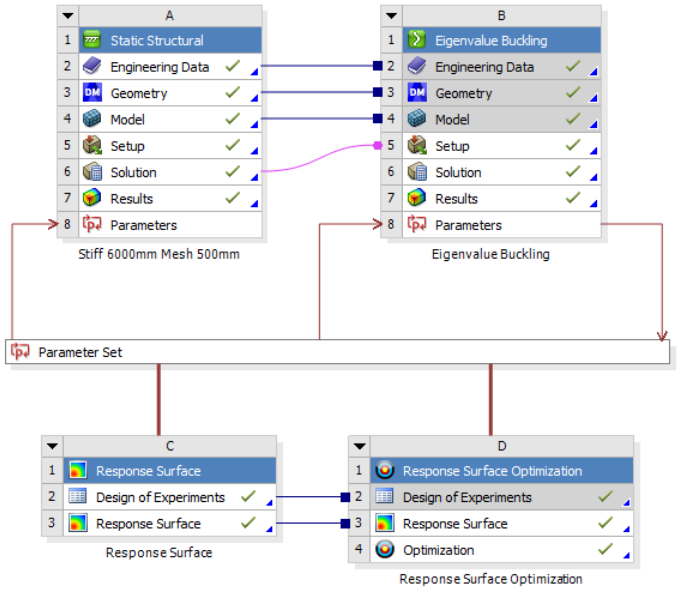

Figure 19 ANSYS General Set-up for Static Structural, Eigenvalue Buckling, and Response Surface

Typically, setup begins by configuring the subsea shuttle geometry and dimensions in the Static-Structural analysis tool. The Design-Modeler feature is used to input geometry dimensions and determine which parameters to examine. Furthermore, the Static-Structural Model feature is used to arrange the boundary conditions, configure the working load, and determine the simulation type that are required to obtain the desired output. In general, the Static-Structural analysis tool is used to ensure that the configured model is theoretically proven to be statically stable and is able to withstand the working load.

As mentioned in sub-chapter 2.3.2, this thesis project will use a linearized approach to study the bifurcation buckling on the subsea pressure hull. Therefore, the Eigenvalue Buckling analysis tool is selected. After the static-structural output is proven to be able to withstand the workload, and then this result will become an input for Eigenvalue Buckling analysis. This feature will generate the total deformation load multiplier which will be used to calculate critical buckling pressure later on. The Buckling Eigenvalue analysis tool can also visualize the possible buckling modes for a configured model.

Prior to the response surface execution; parameter screening is performed to confirm that the selected parameter set represents the parameters that have a significant effect on the model. Parameter screening can be done using Parameter Correlation. After parameter screening is complete, the selected parameter will be used as input in the DoE. The quality of the parameter set in the DoE will determine the quality of the response surface. The response surface is carried out to improve the quality of the response surface estimated values; hence the estimated value will be closer to the measured value. Lastly, the best result from response surface type comparison will be optimized further. This optimization setting can be adjusted to get the optimum value of the desired parameter. For example, by lowering the cylinder dimensions to its lower limit and maximizing the load multiplier as output, ANSYS will generate the other optimum parameters to accommodate these requirements.

4.1.2 MATLAB

DNVGL-RU-NAVAL Part 4 Chapter 1 [17] provides a series of formulas to study the buckling phenomenon on the submersible shell. This thesis project will use this series of formulas to study the failure that may occur in the subsea shuttle pressure hull. It is convenient to use MATLAB software to execute the complex formulas.

By using the same dimensions, boundary conditions, and loads referring to tables 3, 4, and 6, MATLAB will generate an output series indicating the plastic-elastic bending load. The input parameter values are randomly set within limited range; the trend of output parameter values can be obtained. The values and distribution which indicate the relationship of each important inputs and output parameter will be visualized using a scatter diagram.

The results of this numerical experiment will be compared with the trend produced by the ANSYS experimental experiment. However, the output parameter generated by the ANSYS Eigenvalue Buckling analysis tool is still in the total deformation load multiplier value. Thus, to get the same view as the critical buckling pressure, equation 36 from sub-chapter 2.3.2 will be used. Critical buckling pressure is the multiplication product of the external hydrostatic pressure acting on the shell with the total deformation load multiplier. After the output parameters from the ANSYS have become the same form, the trend between each parameter input and parameter output can be displayed in the form of a scatter diagram. MATLAB will help to visualize the relation plot between these parameters. The comparison between MATLAB elastic-plastic buckling pressure and ANSYS critical buckling pressure will be discussed in chapter 5.

4.2 General Specification

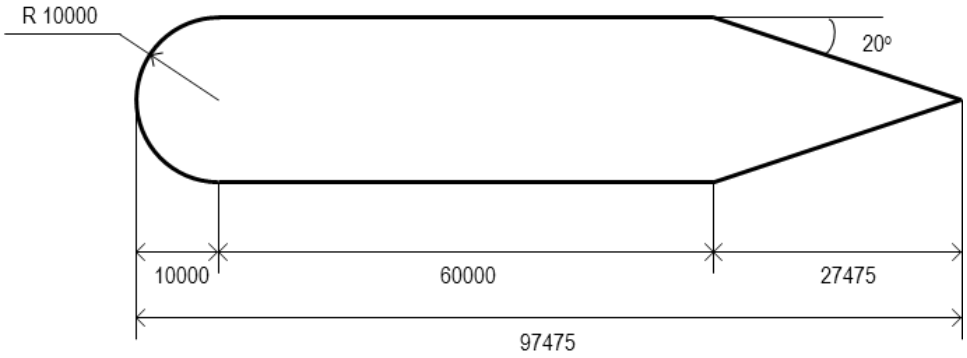

Figure 20 Basic configuration of the Subsea Shuttle pressure hull

The subsea shuttle in this project has the general configuration as shown in the Figure 20. In order to simplify the simulation, the geometry of the subsea shuttle is following the ideal shape with the configuration of cylindrical shell connected to the spherical domes which acting as a bow, and fully conical shape at the other end. Detailed dimension of this configuration shows in Table 3.

Table 3 Subsea Shuttle Dimension

Property	Value	Unit
Dome (Bow) radius	10000	mm
Cylindrical length	60000	mm
Conical (Aft) length	27475	mm
Conical angle	20	degree
Overall subsea shuttle length	97475	mm

The subsea shuttle in this thesis project is designed using a ring-reinforced shell. The ring configuration used will follow the instructions in DNVGL-RU-NAVAL Part 4 Chapter 1 [17]. Details of the ring stiffeners configuration and dimensions can be seen in Figure 21 and Table 4.

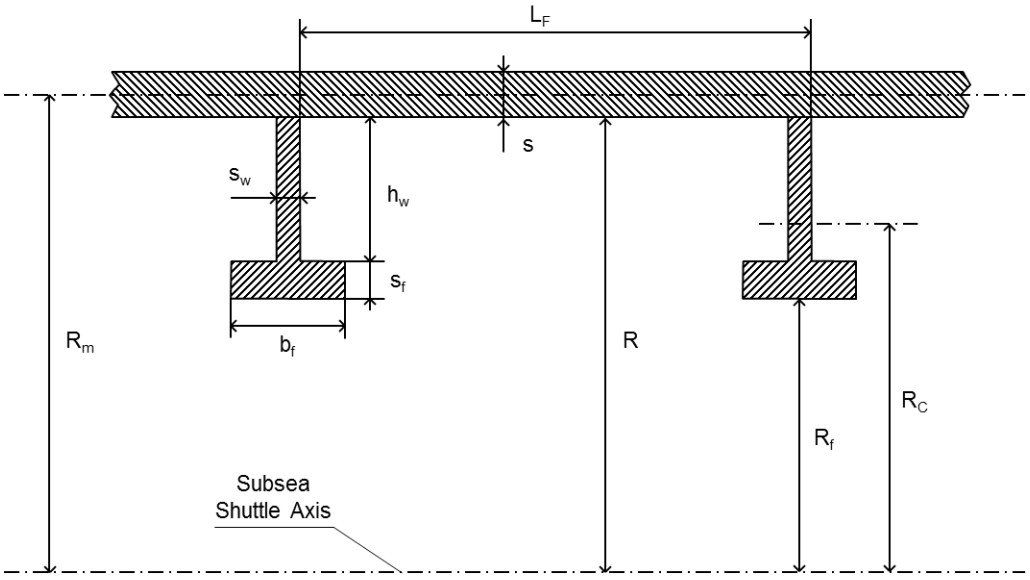

Figure 21 Ring stiffeners konfiguration based on DNVGL-RU-NAVAL Part 4 Chapter 1

Table 4 Ring stiffeners dimension

Property	Symbol	Value	Unit
Cylindrical shell mean radius	R_m	10000	mm
Internal radius of the cylindrical shell	R	9967.5	mm
Cylindrical shell nominal wall thickness	s	65	mm
Web height of the frame	h_w	640	mm
Web thickness of the frame	s_w	15	mm
Flange width of the frame	b_f	268	mm
Flange thickness of the frame	s_f	15	mm
Frame spacing	L_F	6000	mm
Radius to the center of gravity of the frame cross section	R_C	9734.5	mm
Inner radius to the flange of the frame	R_f	9512.5	mm

4.3 Material Properties

The material used in the subsea shuttle pressure hull configuration is assumed to be the same for the cylindrical, spherical, conical, and stiffening rings. The material properties used are linear-elastic steel with the following specifications.

Table 5 Subsea shuttle pressure hull material properties

Parameter	Symbol	Value	Unit
Young's Modulus	E	2.0E+05	N/mm^2
Poisson's Ratio	ν	0.3	
Yield Strength	σ_y	250	N/mm^2
Density	ρ	7.85E+06	kg/mm^3

4.4 Load and Boundary Condition

The nominal load values used in this pressure hull study are presented in the table 6.

Table 6 Nominal load values

Parameter	Symbol	Value	Unit
Force	F	1.8E+06	N
Pressure	P	1	MPa

The boundary condition is useful to limit the analysis under ranged value to achieve a convergence output. There are two loads that are applied as boundary conditions in this experiment. The first boundary condition is the compression load. The external hydrostatic pressure (Point B) acting on the subsea shuttle pressure hull is assumed to be uniform and evenly distributed over the shell surface. The second boundary condition is axial load. A force is applied to the free end (Point C) of the pressure hull in the direction opposite the fixed point. The position and direction setting of the acting force aims to limit the movement of the shell, thus easier to observe. The displacement (Point A) boundary condition is located on the conical shell with the restraint arrangement on the y and z axes, while the shell is free to move in the x-axis. The last boundary condition is fixed support (Point D) which located on the domes shell. This arrangement is to limit shell movement in the three orthogonal directions. Figure 22 shows the boundary conditions applied in this experiment.

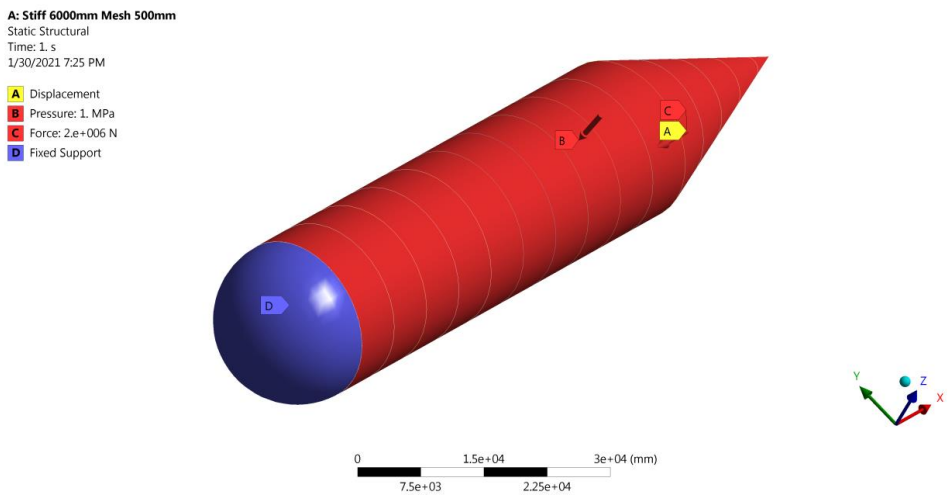

Figure 22 Pressure hull load and boundary conditions

4.5 Preliminary Study

4.5.1 Operational Requirement

As an alternative hydrocarbon transportation system, the subsea shuttle is expected to be able to operate in a certain depth. However, along with increasing depth, an underwater vehicle will also require an increase in all its supporting systems. For example, the necessity for a higher power to get the same speed. Burcher *et al* [6] discussed the minimum depth requirement is such that all of the parts of the submarine is completely submerged. In addition from the operability point of view, the submarine must be able to dive deep enough to avoid collision with other ship draughts. The largest supertanker Seawise Giant has a draught 24.6 m. Therefore, the subsea shuttle in general must have a minimum operating depth of more than 30 m. To be safe, the subsea shuttle in this report is designed to at least be able to operate to a depth of 100 m.

The table 7 below shows the subsea shuttle simulation results regarding the depth of the subsea shuttle operation. The hydrostatic pressure is calculated assuming the subsea shuttle operates in salt water.

$$P = \rho . g . h \qquad \text{(Eq. 46)}$$

Where, $\rho = 1023.6\ kg/m^3$

$g = 9.8\ m/s^2$

It can be seen that with the selected basic dimensions (based on table 3 and 4), the resulting load multiplier and the critical buckling pressure move linearly with the operating depth.

Table 7 Operating Depth Scenarios

Scenario	Depth (m)	Pressure (MPa)	Total Deformation Load Multiplier	Critical Buckling Pressure (MPa)
1	1	0.01	104.52	1.0452
2	50	0.5	2.1147	1.0574
3	100	1	1.0575	1.0575
4	150	1.5	0.7050	1.0575
5	200	2	0.5288	1.0576

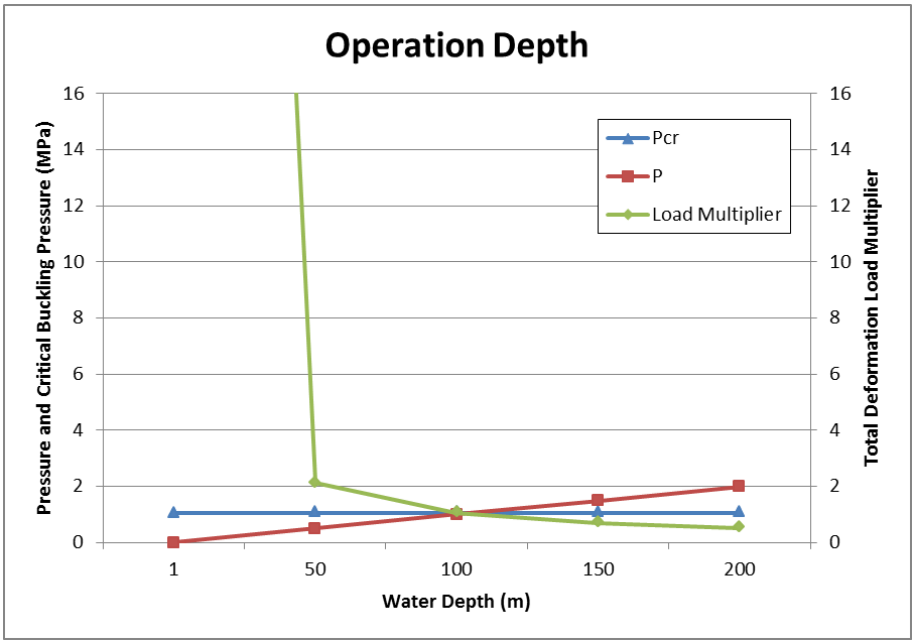

Figure 23 Operation depth comparison

Considering the above results and the demands of the subsea shuttle operation, for further simulation this project will use a pressure of 1 MPa as the external hydrostatic load.

4.5.2 Mesh Refinement Study

In order to validate that the results of analyses are sufficient, mesh refinement study is necessary to be completed. This project evaluates the failure possibility on the shell of the subsea shuttle pressure hull. Hence, the selected mesh setting in this project is face-sizing focused on the shell surface. The refinement study shows in Table 8.

Table 8 Mesh refinement study cases

Mesh Size (mm)	Nodes	Element	Total Deformation Load Multiplier	Critical Buckling Pressure (MPa)
400	41465	49571	1.0323	1.0323
425	35676	36635	1.0594	1.0594
450	32958	38764	1.0419	1.0419
475	28624	34925	1.0548	1.0548
500	27250	32110	1.0538	1.0538
525	23907	24376	1.0267	1.0267
550	21184	25252	1.0960	1.0960

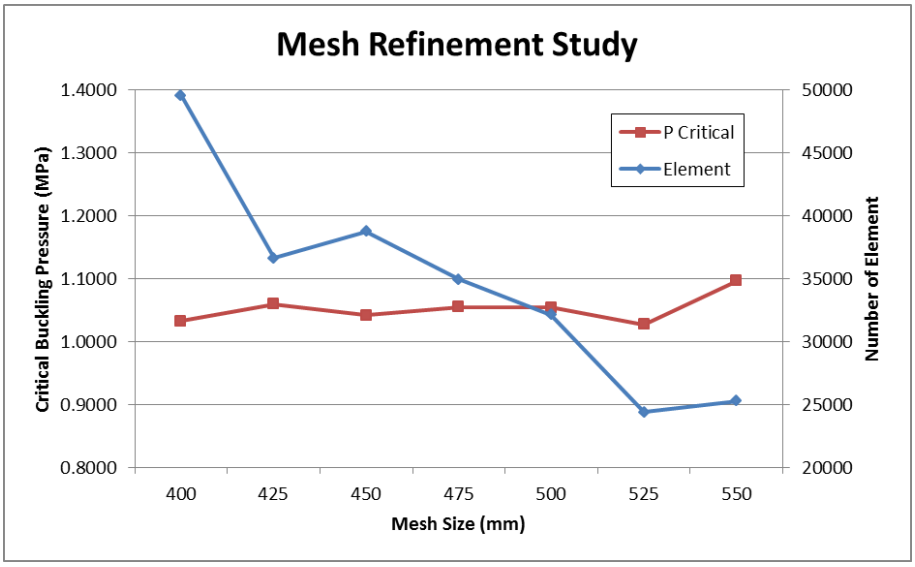

Figure 24 The comparison of mesh refinement study cases

The results show that the total deformation load multiplier which acts as the main failure indicator is stable at mesh size 425 mm up to 500 mm. The 425 mm mesh will give more accurate results. However, given the large dimensions of the pressure hull and to reduce the experiment time with an acceptable efficiency, the project will use a mesh size of 500 mm.

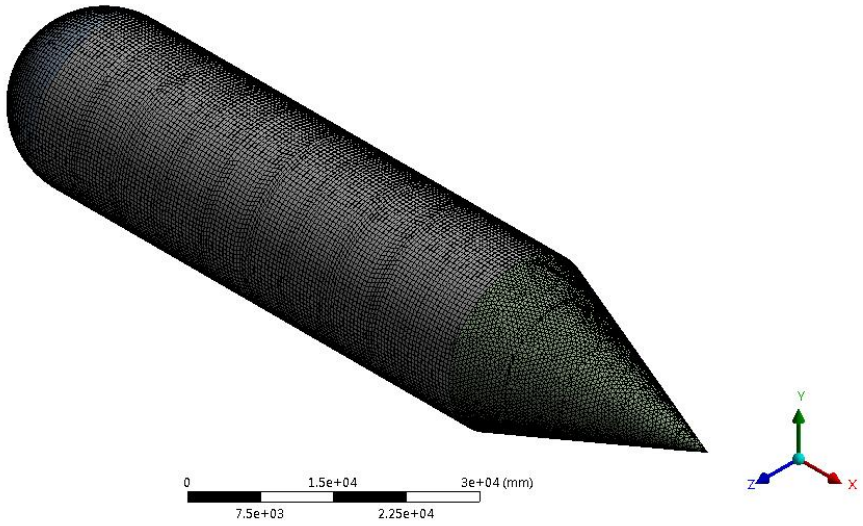

Figure 25 Face sizing with mesh size 500 mm

4.5.3 Frame Spacing Study

The ring stiffeners used in this project are designed with a certain distance. In order to study the characteristics of the distance between the two stiffening rings and their effect on the output parameters, this experiment was carried out.

Table 9 Frame Spacing

Frame Spacing L_F (mm)	Total Deformation Load Multiplier	Critical Buckling Pressure (MPa)
3000	1.6098	1.6098
4000	1.3210	1.3210
5000	1.1884	1.1884
6000	1.0538	1.0538
7500	0.9133	0.9133
10000	0.6926	0.6926

Experiment was executed by varying the number of stiffening rings and placing them evenly on the cylindrical shell of the same length. This experiment will generate variations in the total deformation load multiplier. Figure 26 shows the density variation for each frame configuration.

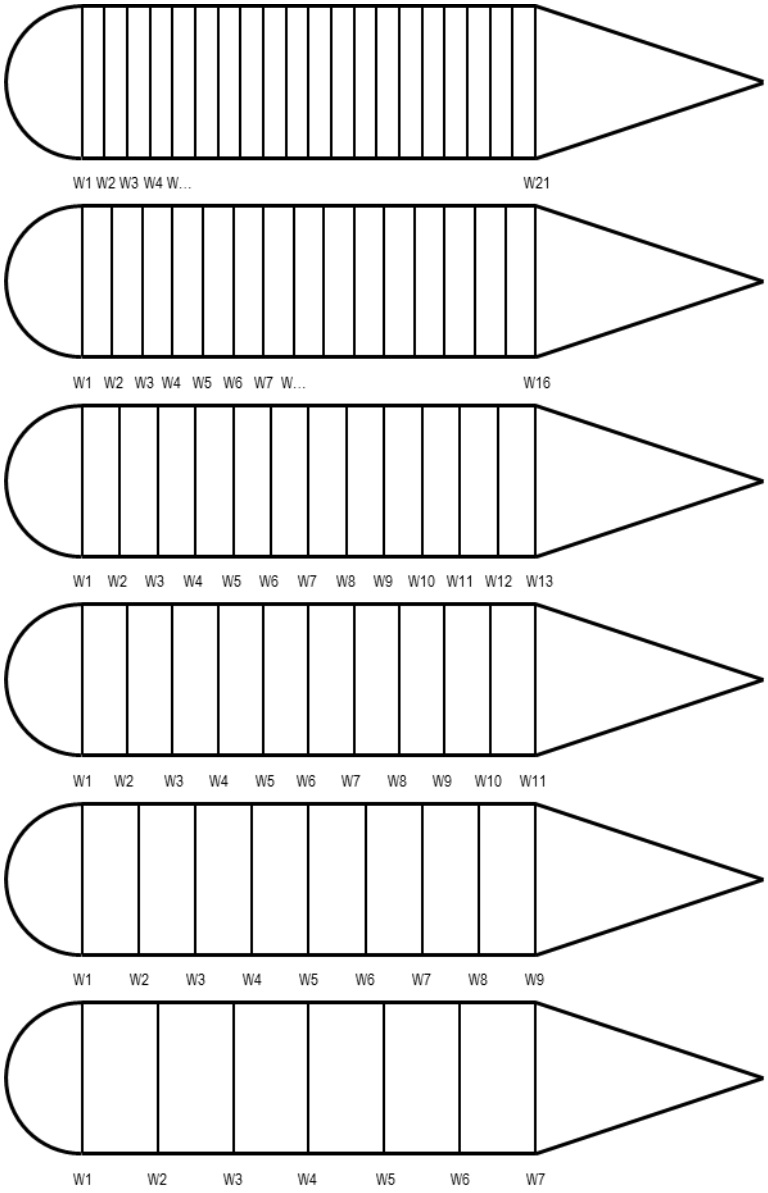

Figure 26 Frame spacing variations on cylinders of the same length.

The results shown in Table 9 indicate that the wider the distance between the frames or the fewer frame amounts resulted in the smaller the total deformation load multiplier. The load multiplier corresponds to the critical buckling pressure the shell can withstand. Thus, with a critical pressure smaller than the hydrostatic pressure, the shell will buckle.

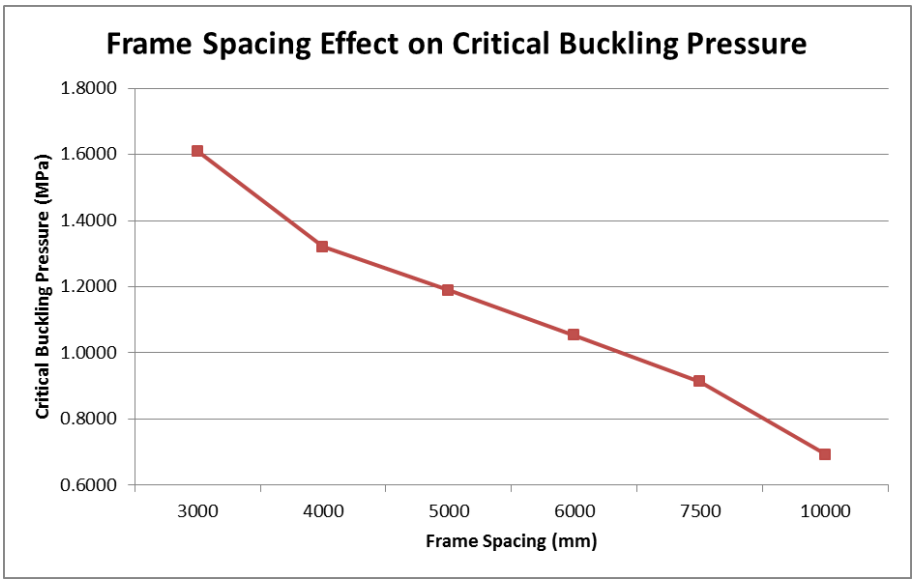

Figure 27 The frame spacing effect on critical buckling pressure

Based on the experimental results, frame spacing with a distance of 7500 mm or longer is not applicable. Whereas a shell with frame distance of 6000 mm or shorter are proven to be able to withstand hydrostatic loads. In general, it can be said that the denser the distance between the frames, the stronger the shells will withstand critical loads. For a more conservative experiment, this project will use a frame spacing of 6000 mm.

Using the same principle, frame spacing applied to the conical shell will use the same frame spacing as the cylindrical shell.

4.5.4 Buckling Mode Observation

During the simulation, several buckling modes can be observed. The buckling mode that occurs is influenced by the configuration and dimensions of the structure. Some of the observed buckling modes are shown below:

- Asymmetric buckling / lobar buckling / local buckling

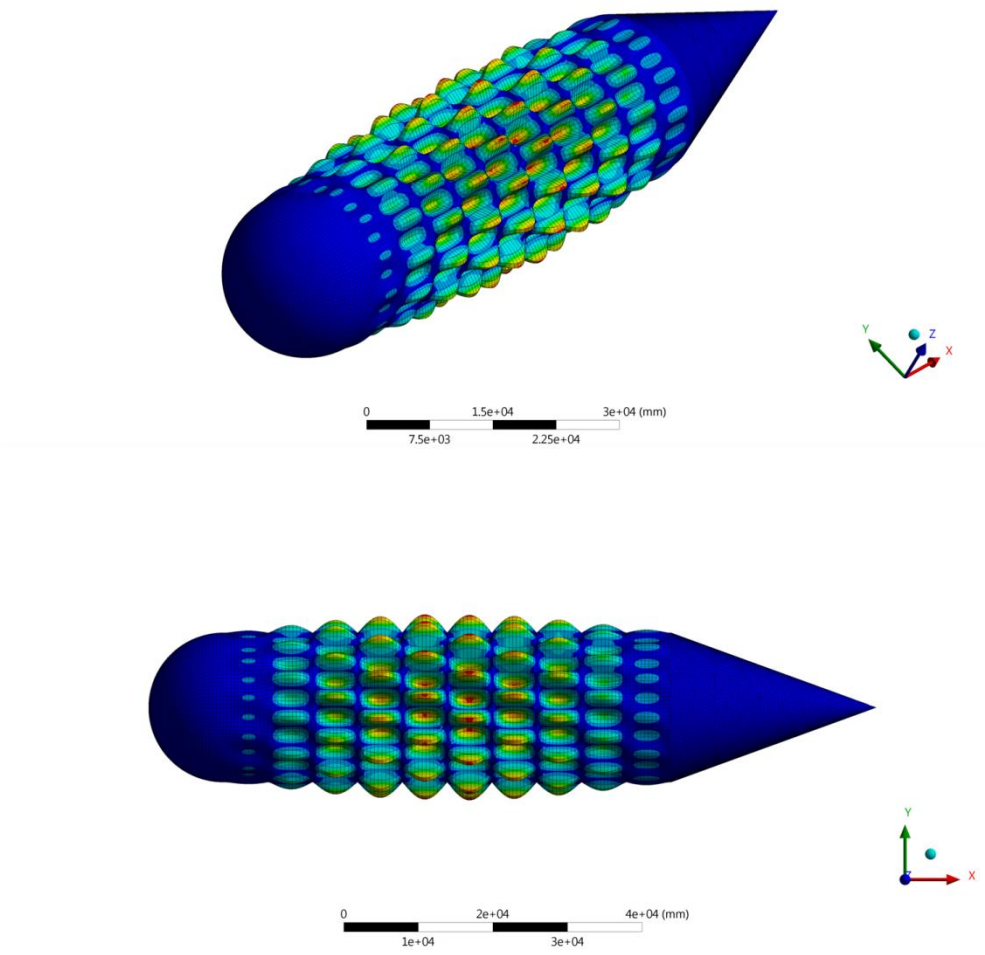

Figure 28 the asymmetric collapse on pressure hull.

Table 10 The pressure hull main parameter (in mm.) dimension during asymmetric collapse

Rm	hw	bf	s
10000	640	268	45

If the ring-reinforced stiffeners are rigid enough to be able to withstand the critical load, the unsupported shell will buckle.

- General instability of shell and ring / overall buckling / global buckling

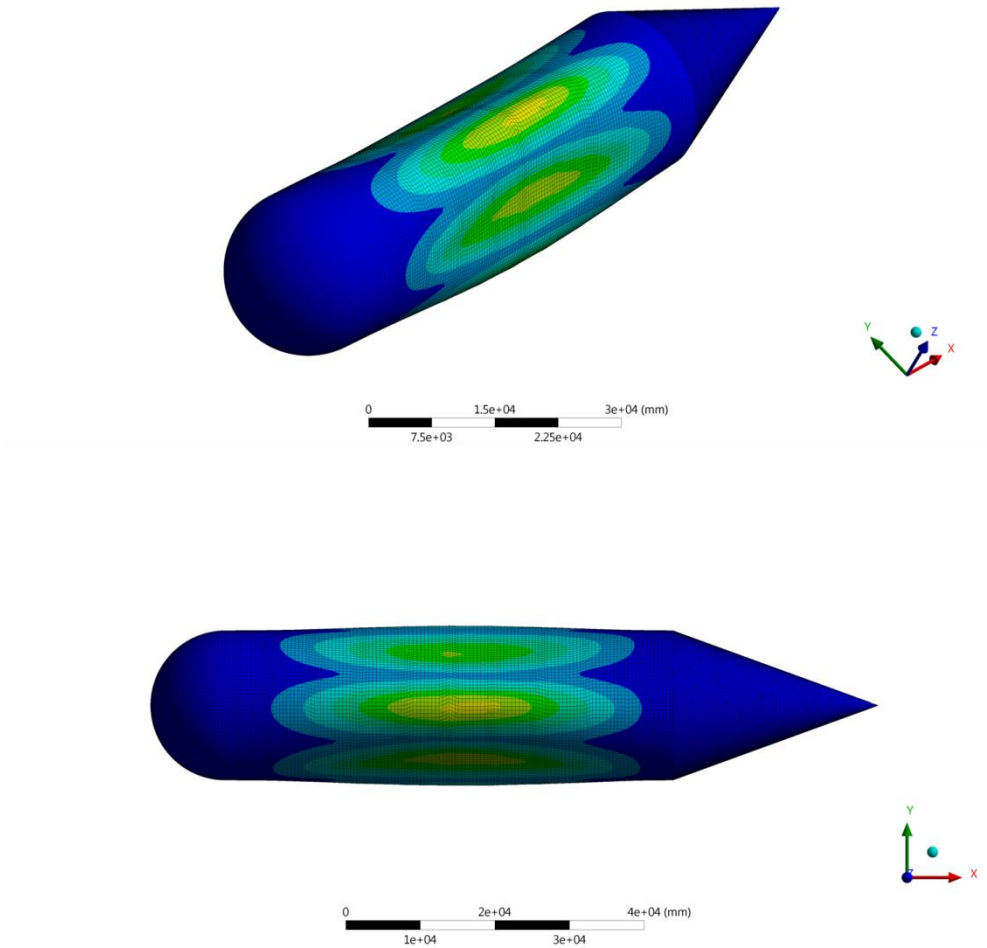

Figure 29 Global buckling on the pressure hull

Table 11 The pressure hull main parameter (in mm.) dimension during global buckling

Rm	hw	bf	s
10000	640	268	65

The ring-reinforced shell under external pressure may buckle if the supported rings are considered weak or light in comparison to the shell [18].

- Frame Buckling

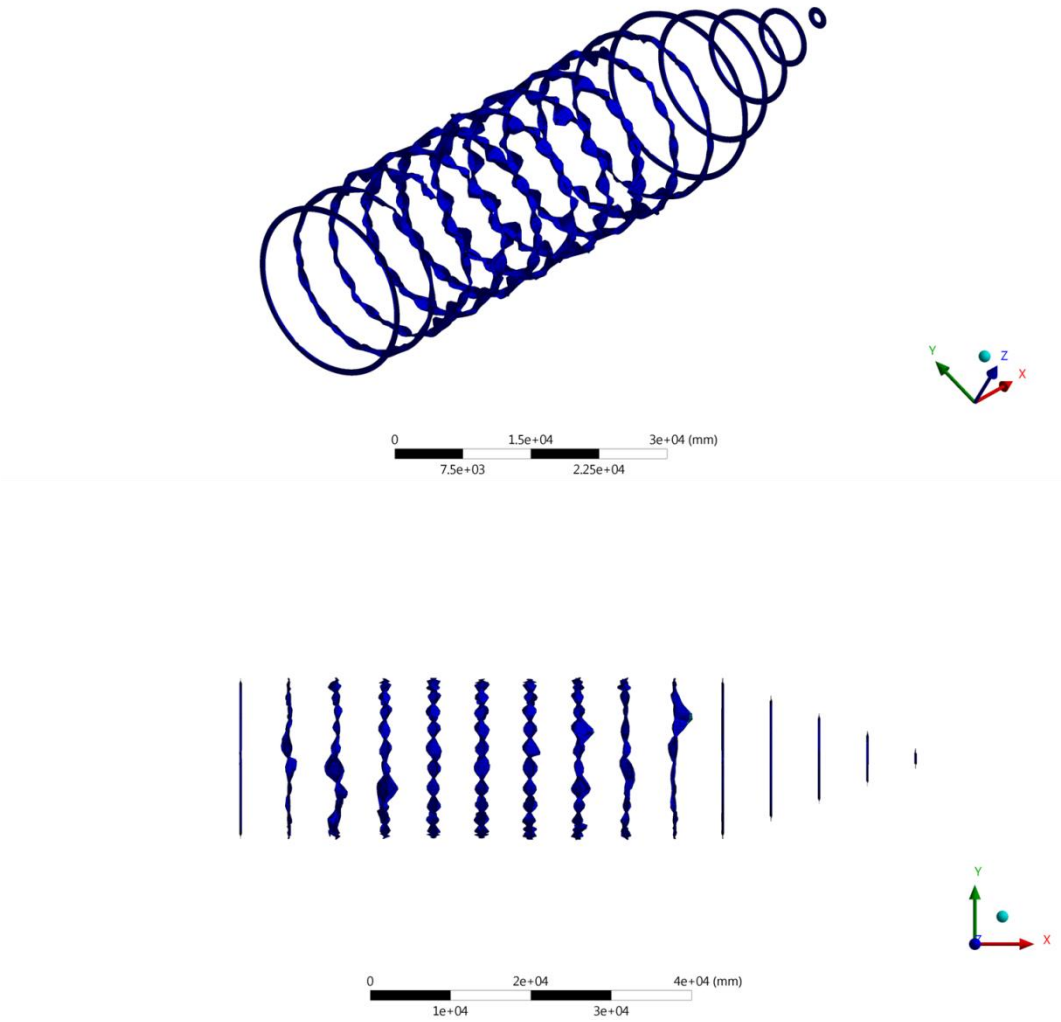

Figure 30 Frame Buckling

Table 12 The pressure hull main parameter (in mm.) dimension during frame buckling

Rm	hw	bf	s	sw, sf
10000	640	268	45	10

- Frame Buckling

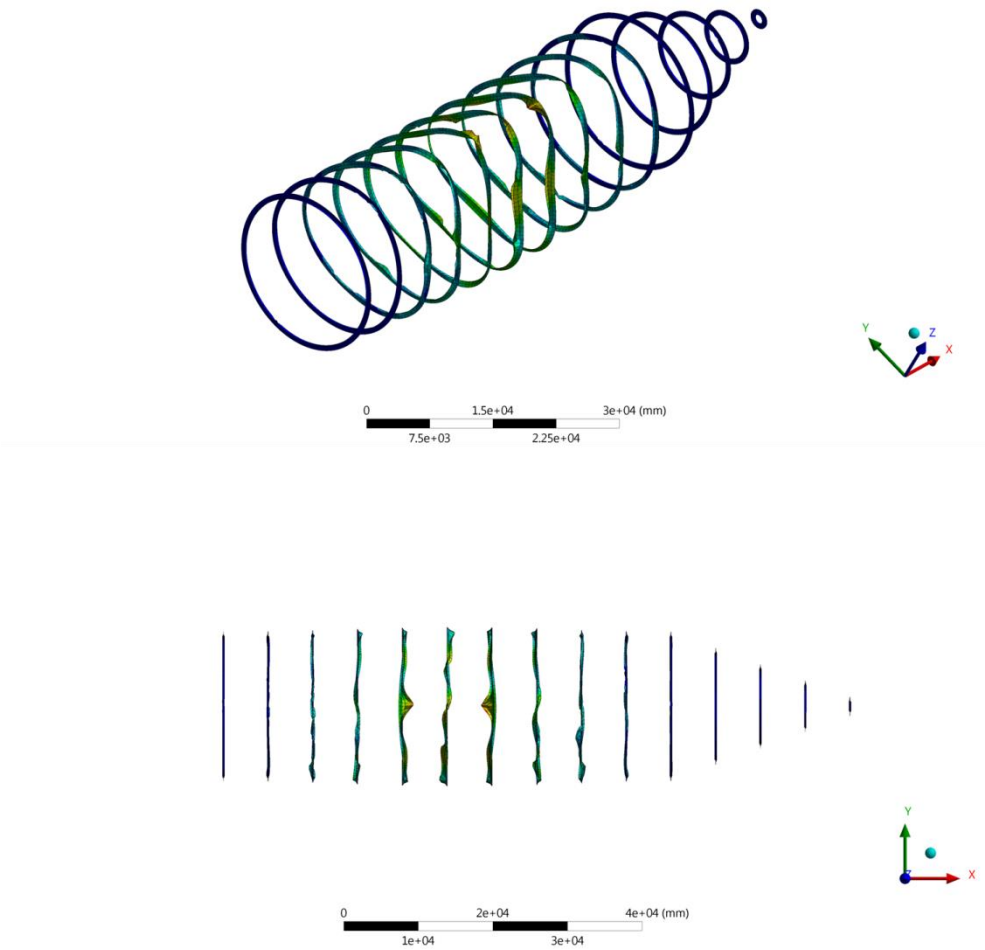

Figure 31 Tripping

Table 13 The pressure hull main parameter (in mm.) dimension during tripping

Rm	hw	bf	s	sw, sf
10000	640	268	65	10

4.5.5 Range of Selected Parameters

To understand the effect of a parameter on other parameters, a data distribution that represents the relationship between the two parameters is required. In order to generate distribution, each parameter needs to set a lower limit and an upper limit. The following table 14 shows the value limit for each parameter.

Table 14 Range of the pressure hull parameter

Parameter	Symbol	Lower Bound	Upper Bound	Unit
Cylindrical Mean Radius	Rm	9150	10850	mm
Web Height	hw	576	704	mm
Flange Width	bf	241.2	294.8	mm
Cylindrical Wall Thickness	s	58.5	71.5	mm
Bow Wall Thickness		58.5	71.5	mm
Aft Wall Thickness		58.5	71.5	mm
Web Thickness	sw	13.5	16.5	mm
Flange Thickness	sf	13.5	16.5	mm
Aft Web Thickness		13.5	16.5	mm
Aft Flange Thickness		13.5	16.5	mm
Pressure	P	0.9	1.1	MPa
Force	F	1.8E+06	2.2E+06	N

5. Discussion

5.1 Parameter Correlation

5.1.1 Parameter Screening

To find out which parameters have a major influence on a design, a structured methodology is required. Using the ANSYS Workbench 2020, the Spearman parameter correlation and determination method was chosen to investigate a number of parameters of the pressure hull. The input and output parameters arrangement in the correlation parameter analysis can be seen in the table 15 below.

Table 15 Parameter Correlation Arrangement

No	Input Parameter Static Structural	
1.	P1 – Rm	Geometrical Properties
2.	P2 – hw	
3.	P3 – bf	
4.	P4 – Wall Thickness	
5.	P5 – Bow Thickness	
6.	P6 – Aft Thickness	
7.	P7-P17 – Web Thickness	
8.	P18-P28 – Flange Thickness	
9.	P29-P32 – Aft Web Thickness	
10.	P33-P36 – Aft Flange Thickness	
11.	P37 – Pressure Magnitude	Boundary Load
12.	P38 – Force Magnitude	

No	Output Parameter Eigenvalue Buckling	
1.	P40 – Total Deformation Load Multiplier	Eigenvalue Buckling

A linear correlation matrix based on Spearman methodology with a size of N=100 samples is shown in the Figure 32.

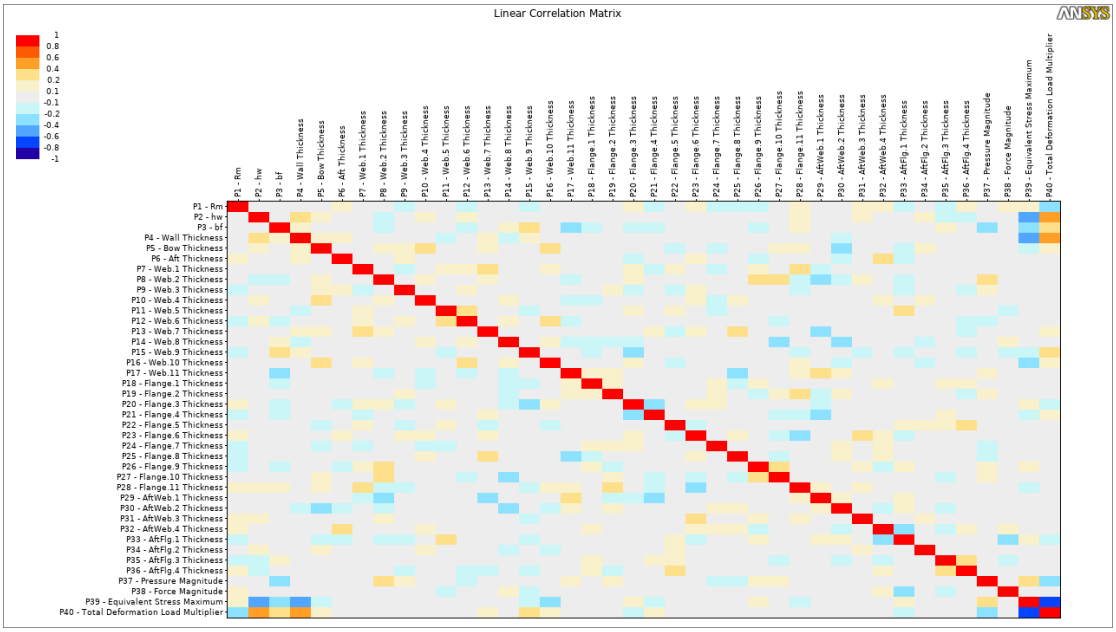

Figure 32 Linear Paramater Correlation Matrix with sample size N=100

In the obtained linear correlation matrix, there was no observed strong relationship between the parameters involved. The coefficients acquired vary and spread throughout the matrix. However, there are a few parameters stands out from the rest. The coefficients from this matrix can be mapped and interpreted as follows:

Table 16 Linear Correlation Matrix Interpretation

Parameter	Symbol	Correlation Level Relative to Load Multiplier
Cylindrical Mean Radius	Rm	Low Negatif Correlation
Web Height	hw	Low Positif Correlation
Flange Width	bf	Low Positif Correlation
Cylindrical Wall Thickness	s	Moderate Positif Correlation
Bow Wall Thickness		Negligible Correlation
Aft Wall Thickness		Negligible Correlation
Web Thickness	sw	Negligible Correlation
Flange Thickness	sf	Negligible Correlation
Aft Web Thickness		Negligible Correlation
Aft Flange Thickness		Negligible Correlation
Pressure	p	Low Negatif Correlation
Force	F	Negligible Correlation

To have a better understanding of the correlation between the parameters involved, the parameters that have at least a low interpretation coefficient will be presented in more detail in Figure 33.

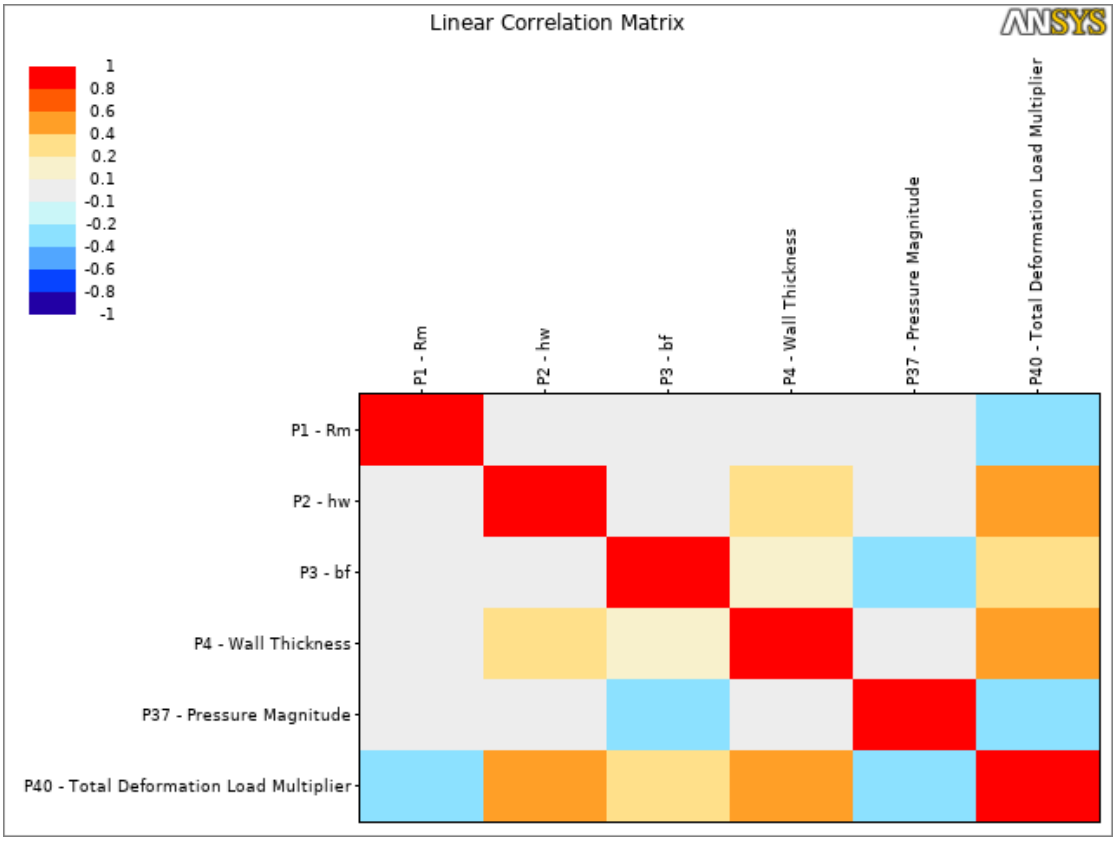

Figure 33 Selected parameters linear correlation matrix

The matrix for the selected parameters shown in Figure 33 can also be displayed in tabular form.

Table 17 Selected parameters linear correlation matrix in tabular form

	P1 – Rm	P2 – hw	P3 – bf	P4 – s	P37 – P	P40 - λcr
P1 – Rm	1	0.0087	-0.0708	0.0096	-0.0357	-0.3514
P2 – hw	0.0087	1	-0.0074	0.2123	0.0467	0.4390
P3 – bf	-0.0708	-0.0074	1	0.1408	-0.2347	0.3790
P4 – s	0.0096	0.2123	0.1408	1	-0.0350	0.5800
P37 – P	-0.0357	0.0467	-0.2347	-0.0350	1	-0.3753
P40 - λcr	-0.3514	0.4390	0.3790	0.5800	-0.3753	1

From table 17 it can be observed the manners of each parameter toward the others. The cylindrical wall thickness as represents by P4 shows a moderate positive correlation toward the load multiplier. Since the total deformation load multiplier corresponds to critical buckling pressure, it means with the increasing cylindrical shell wall thickness, the critical buckling pressure will increase as well. This also can be said that the pressure hull shell will perform better against the hydrostatic load. Moving on to the other relations, cylindrical wall thickness has a low to almost negligible correlation to the other parameter inputs.

Additionally, the other inputs have low interpretation toward load multiplier. However, it can be observed that the cylindrical radius provides a different correlation direction compared to other input parameters. If the other parameters have a positive correlation toward the load multiplier, then the cylindrical mean radius has a negative correlation with the load multiplier. This means along with the increasing pressure hull radius, the load multiplier will decrease. It can also be said that the bigger the pressure hull radius, the smaller the resistance to hydrostatic pressure, leads to early failure.

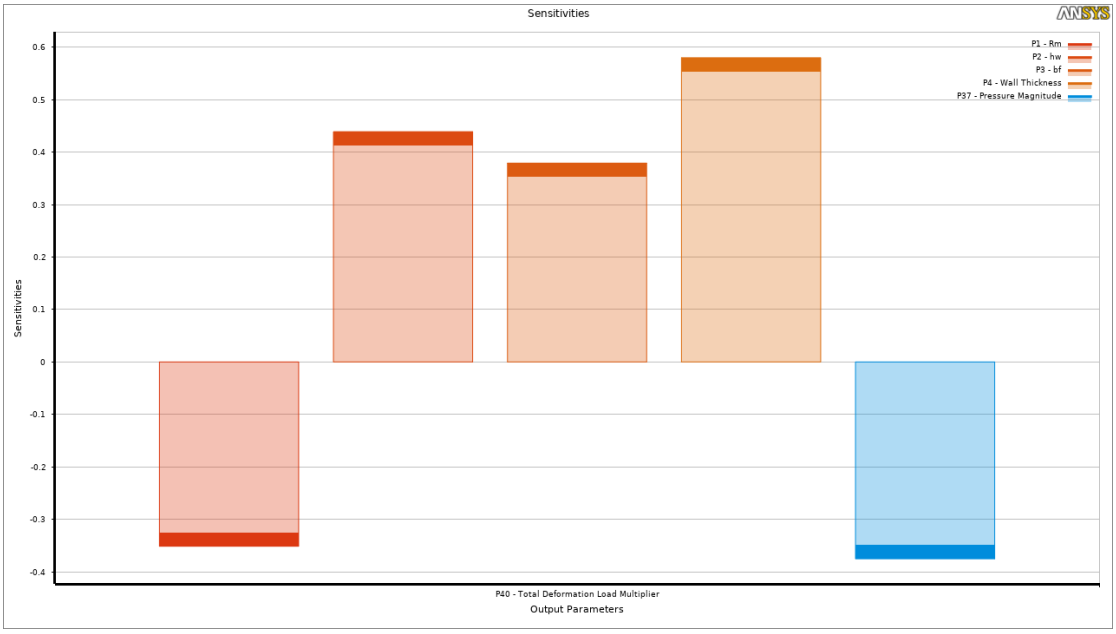

Figure 34 Parameter Sensitivity

Figure 34 shows the sensitivity of the selected parameters against the total deformation load multiplier. The Figure also in accordance with the interpretation listed in table 16. Additionally, the chart also indicates that cylindrical shell wall thickness holds an important aspect in hull design.

The mapping result of the parameter correlation level is also strengthened by the sensitivities chart shown in the Figure 34. It can be seen that the following parameters have a significant effect on the total deformation load multiplier.

- Cylindrical Mean Radius (R_m),
- Web Height (h_w),
- Flange Width (b_f)
- Cylindrical Wall Thickness (s)

Therefore, next analysis in this project will only focus on these four parameters.

5.1.2 Influence of Design Parameter

The following discussions are still based on the Design Point data generated by Parameter Correlation. The Design Point on the ANSYS Workbench contains a series of input parameter data which is generated randomly by the ANSYS algorithm taking into account all the existing constraints. Furthermore, ANSYS will process this randomized input parameters using the selected parameter correlation method. Output data in response to input parameters will be written to the Design Point table until all input parameter has been processed and the experimental series reaches a convergent state.

Data input and output parameters contained in the design point are presented in various forms. One of them is a scatter diagram which illustrates the distribution of the relation between input and output parameters. On this occasion, the input parameter that influence the output according to the screening carried out in the previous stage will be plotted using MATLAB software so that it can be compared with the calculated data based on the formula from DNVGL-RU-NAVAL Part 4.

Cylindrical Mean Radius effect on Buckling Pressure

This experiment will compare the effect of cylindrical radius on elastic-plastic buckling pressure obtained from the MATLAB simulation against the effect of cylindrical radius on critical buckling pressure from ANSYS Design Point data.

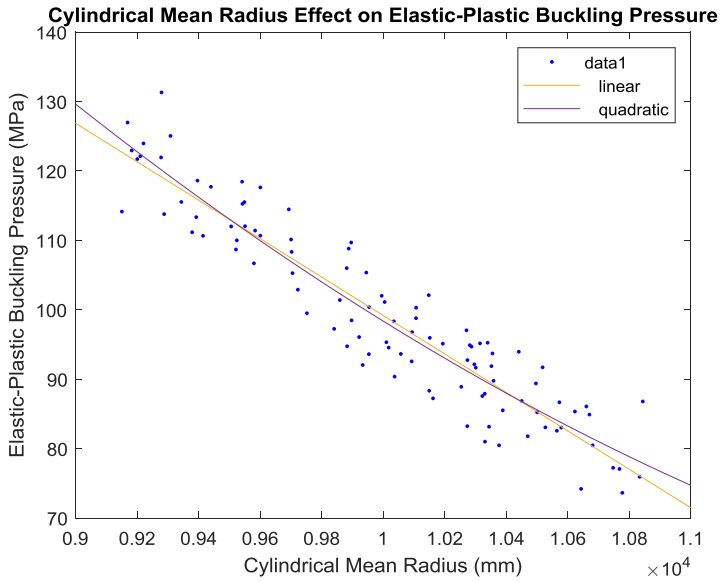

Figure 35 Cylindrical Radius vs Elastic-Plasctic Buckling Pressure, based on DNVGL formula and MATLAB

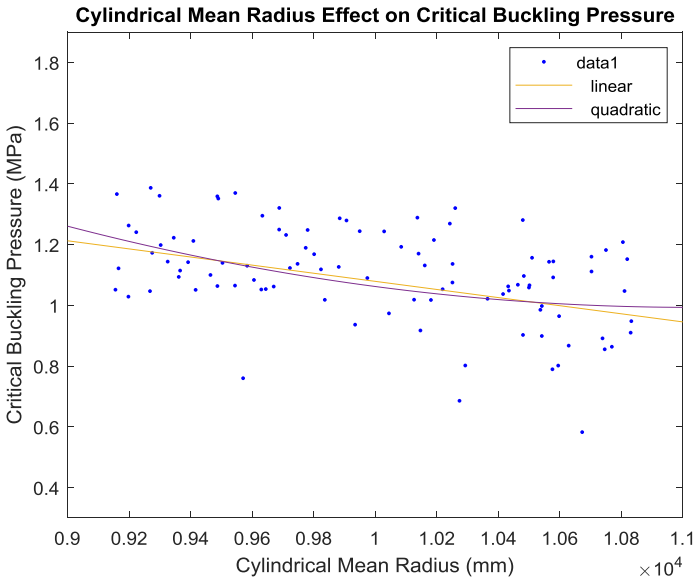

Figure 36 Cylindrical Radius vs Critical Buckling Pressure, plotted from ANSYS Design Point

Comparing the results of the calculation of the MATLAB (Figure 35) with the ANSYS distribution plot (Figure 36) for the effect of the cylindrical shell on the buckling load shows that the cylindrical radius has an effect that is inversely proportional to the critical buckling pressure. This is indicated by the value of the buckling pressure which decreases with increasing cylindrical radius shell. The chart in these two Figures also proves that the interpretation in the linear correlation matrix for cylindrical radius and buckling load has a negative correlation.

Figure 35 shows the cylindrical radius has a large effect on the elastic-plastics buckling load. The slopes shown on this chart indicate that elastic-plastic buckling pressure is very sensitive to changes in the cylindrical radius of the shell. Meanwhile, the slope of the ANSYS chart in Figure 36 is not as sharp as the slope of the cylindrical radius – elastic-plastic buckling curve. This indicates that the effect of the cylindrical radius on critical buckling pressure is not as sensitive as the effect on elastic-plastic buckling pressure. Moreover, the correlation interpretation between the two is considered low.

It can also be observed that the value of elastic plastic buckling is much greater than the value of critical buckling in the same radius range. This is understandable considering the limit load of the perfect shell (theoretical) is much higher than the limit load of the imperfect shell (ANSYS or computer simulation). The imperfections arising from the choice of geometry can also affect this behavior.

Overall it can be said, the pressure hull shell will be more susceptible to failure due to the hydrostatic loads as the cylindrical radius becomes bigger.

Web Height effect on Buckling Pressure

This experiment will compare the effect of web height on the elastic-plastic buckling pressure obtained from the MATLAB simulation against the effect of web height on the critical buckling pressure from ANSYS Design Point data.

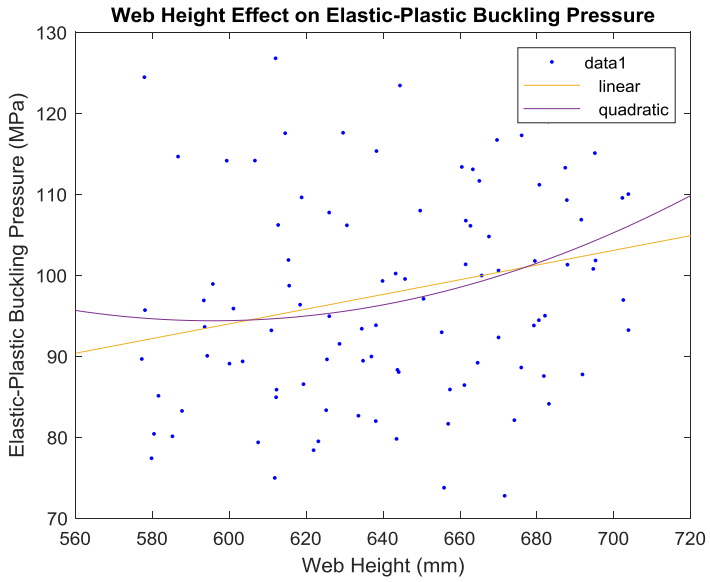

Figure 37 Web Height vs Elastic-Plasctic Buckling Pressure, based on DNVGL formula and MATLAB

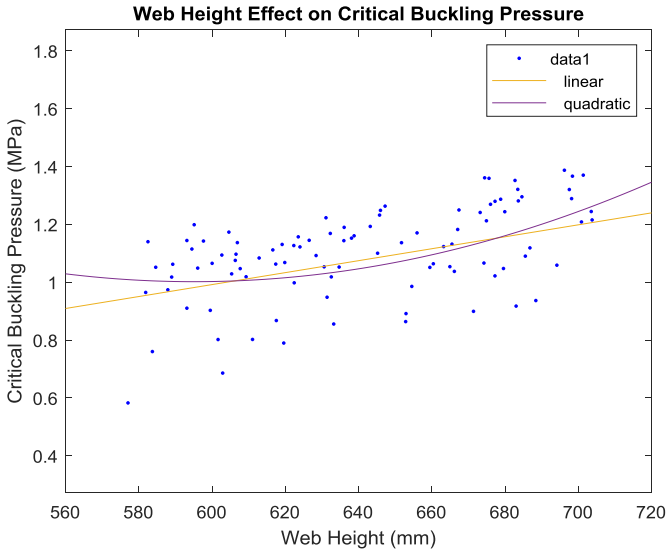

Figure 38 Web Height vs Critical Buckling Pressure, plotted from ANSYS Design Point

From Figure 37 and Figure 38 it can be concluded that the web height has the same effect on the bending pressure of the elastic plastic and the critical bending pressure. Although the value for the elastic plastic bending pressure is higher than the value for the critical bending pressure in the same web height range, it can be said that the relationship between the web height and the two types of loads has a positive weak or low correlation. This is indicated by the slope of the two curves forming the same positive correlation direction. Linear and quadratic fittings to the distribution of these two curvatures also give the same pattern. Hence, the thicker the web on the pressure hull ring stiffeners, the more pressure hull shell can withstand hydrostatic pressure.

The difference in the values of the two pressures can be explained because the limit load on the perfect shell without imperfections has a higher value than the value generated from the computer analysis.

Interestingly in Figure 37, it can be observed that the distribution of the relationship between the web height and elastic-plastic bending pressure is scattered across the graph. This shows that the correlation between these two variables is not very conclusive and may change the direction of the correlation. Relationships that initially have a positive correlation might turn into a negative correlation.

Flange Width effect on Buckling Pressure

This experiment will compare the effect of flange width on the elastic-plastic buckling pressure obtained from the MATLAB simulation against the effect of flange width on the critical buckling pressure from ANSYS Design Point data.

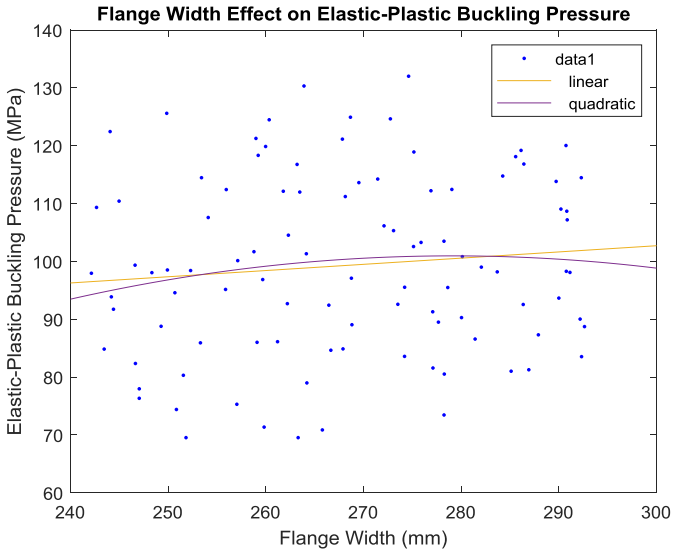

Figure 39 Flange Width vs Elastic-Plasctic Buckling Pressure, based on DNVGL formula and MATLAB

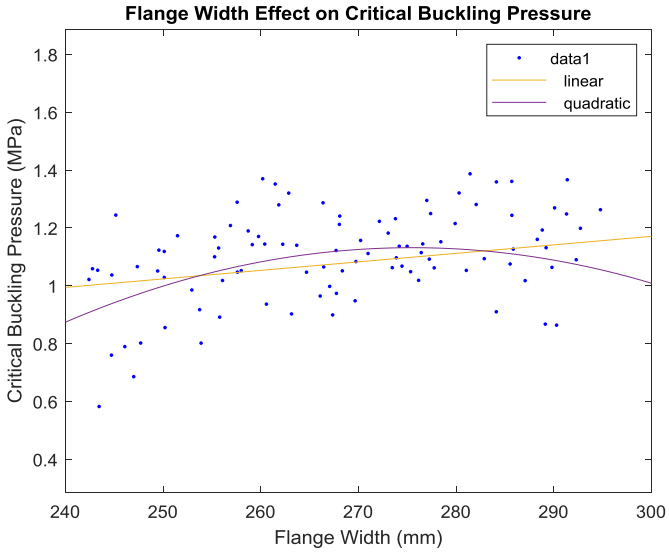

Figure 40 Flange Width vs Critical Buckling Pressure, plotted from ANSYS Design Point

By comparing the two curvatures in Figures 39 and 40, it can be observed that the flange width has the same effect on the elastic-plastic bending pressure and the critical bending pressure. Similarly as observed in the web height, the relationship between flange width and the two buckling pressures has a positive weak or low correlation.

The first indication that the relationship between flange width as input and buckling pressure as output has a weak positive correlation is the degree of slope of the curvature. It can be observed that the lower limit value of flange width gives a smaller response than the response generated by the upper limit value of flange width. The second indication is, linear and quadratic curve fittings have a same direction and curvature which indicates a weak positive correlation between these variables.

The spread of responses for the relation of flange width and critical buckling pressure is more coherent and clearly shows the positive slope direction of the correlation. However, the same cannot be said for the relation of flange width to elastic-plastic bending stress. The spread that represents the relation of these two parameters is comprehensive throughout the chart. Hence, the interpretation of the relation between these two variables may not be conclusive.

In general, the pressure hull shell will be more able to withstand hydrostatic loads as the flange on the stiffener ring becomes wider.

Cylindrical Wall Thickness effect on Buckling Pressure

This experiment will compare the effect of cylindrical wall thickness on the elastic-plastic buckling pressure obtained from the MATLAB simulation against the effect of cylindrical wall thickness on the critical buckling pressure from ANSYS Design Point data.

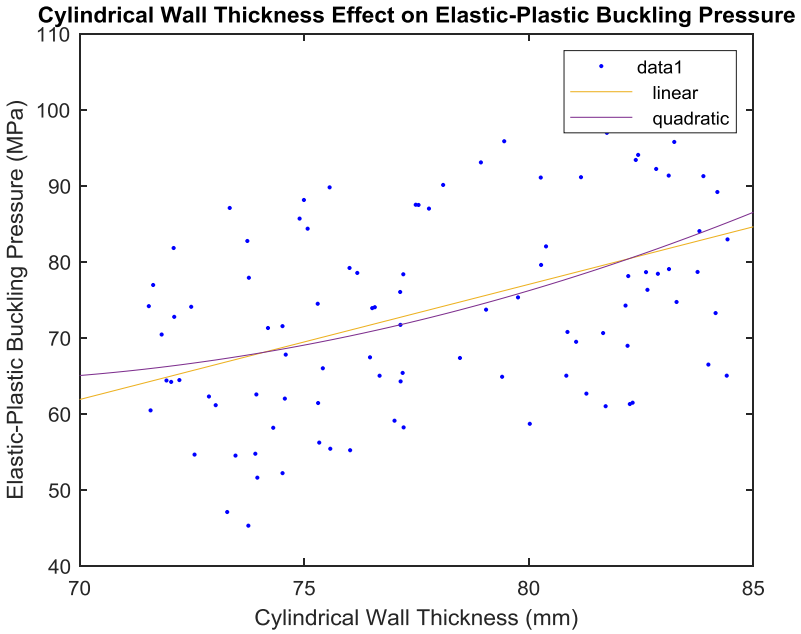

Figure 41 Cylindrical Wall Thickness vs Elastic-Plasctic Buckling Pressure, based on DNVGL formula and MATLAB

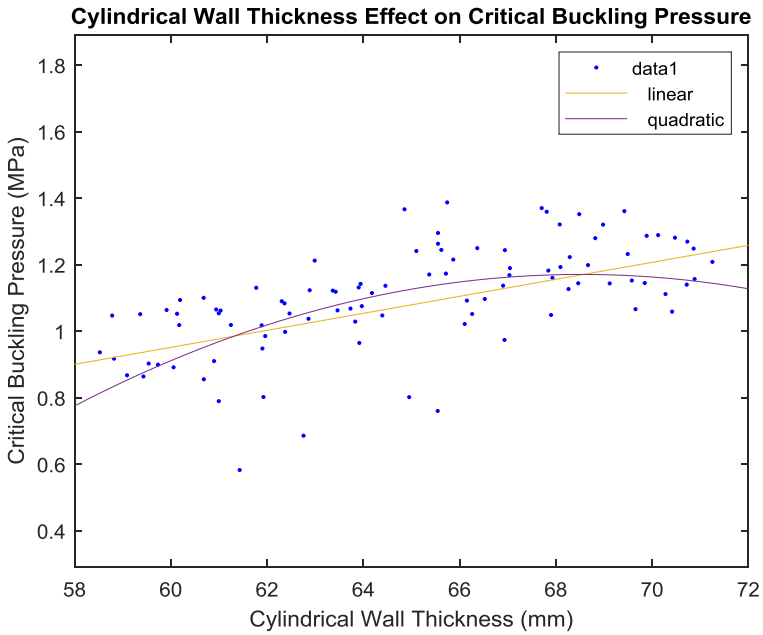

Figure 42 Cylindrical Wall Thickness vs Critical Buckling Pressure, plotted from ANSYS Design Point

The effect of cylindrical wall thickness on bending pressure can be explained based on the two charts in Figures 41 and 42. In general, it can be observed that the relationship between these variables has a positive correlation. However, the indicator of the degree of slope of the curvature on these two charts does not show a sharp enough slope compared to the slope of the curve in the cylindrical radius - elastic-plastic buckling pressure relation in Figure 35. Though, it is also not as flat as the curves of influence of web height and flange width on bending pressure. Thus, it can be said that the relationship between cylindrical wall thickness and bending pressure has a moderate positive correlation. This is in accordance with the interpretation results obtained from readings of the linear correlation matrix in table 16.

The distribution on those two Figures that indicates the relationship between the cylindrical wall thicknesses to the two bending pressures was also coherent. Consequently, the resulting correlation for both curvatures is also conclusive. Hence, the thicker the pressure hull wall, the higher the ability of the pressure hull shells to withstand hydrostatic loads.

Similarly to the behavior of effect of cylindrical radius, web height, and flange width on bending stress, the effect of cylindrical wall thickness on elastic-plastic buckling pressure value has a different value than the effect of cylindrical wall thickness on critical buckling pressure. Observations on these four parameters show that the effect on plastic elastic buckling pressure is generally higher than the effect on the critical buckling pressure. As discussed in sub-chapter 2.3.1, the limit load on the perfect shell which is assumed to be without imperfection is much higher than the critical load limit (computer generated value) and the bifurcation load limit.

The scatter diagrams generated by the ANSYS Workbench for these four parameters are available in Appendix A of this report.

5.2 Response Surface

This experiment uses the ANSYS Workbench 2020 Response Surface tool. This report will discuss five types of response surface methodology and compare the results of the five. The response surface with the estimated value closest to the measured value will be further optimized to determine the optimal capability of the designed geometry.

Based on the results of the parameter correlation study using the Spearman method with a sample size of N = 100, it was found that there are four parameters that have an influence on the ability of the subsea pressure hull to withstand hydrostatic loads. The four parameters are cylindrical mean radius, web height, flange width, and cylindrical wall thickness.

5.2.1 Design of Experiments

As discussed in sub-chapter 3.2, the generated sample data size represents by Design of Experiment (DoE) has a great influence on the response surface predictive value. A large data sample will increase the quality of predictive value and decrease the gap between estimation and real measured value. Response surface type also has an effect on the approximate value. Hence, it is necessary to carefully choose appropriate response surface method to analyze a series of data.

The Design of Experiment sample size was generated automatically by ANSYS based on the input parameter size. The following table is showing DoE size variance.

Table 18 ANSYS generated Design of Experiment Size based on Input Parameter Size

Input Parameter Size	Design of Experiment Size
5	27
10	149
15	287
20	551

Taking into account that there are only four parameters that have a significant effect on the load multiplier and with the aim of increasing the quality of the response, a

number of parameters will be added to increase the number of inputs to size 10. Therefore, the selected parameters for further study in this response surface can be seen in table 19. The lower and upper limits used follow the range which is also used in the study parameter correlation.

Table 19 Parameter Set used in Response Surface

Parameter	Symbol	Lower Bound	Upper Bound	Unit
Cylindrical Mean Radius	Rm	9150	10850	mm
Web Height	hw	576	704	mm
Flange Width	bf	241.2	294.8	mm
Cylindrical Wall Thickness	s	58.5	71.5	mm
Bow Wall Thickness		58.5	71.5	mm
Aft Wall Thickness		58.5	71.5	mm
Web Thickness	sw	13.5	16.5	mm
Flange Thickness	sf	13.5	16.5	mm
Pressure	P	0.9	1.1	MPa
Force	F	1.8E+06	2.2E+06	N

Although pressure and force also act as boundary conditions, considering that the subsea shuttle is designed to be able to operate back and forth at a depth of 0-100 m, it is understandable that these two parameters are also included in the input parameter. However, the detailed discussion remains only focused on the four main parameters that have a big effect on the output.

Prior to discussing DoE, an experiment with base dimensions and without applying variations to the parameters was carried out to obtain the total deformation load parameter. This value represents the ability of the pressure hull to be able to withstand hydrostatic loads. Given that at a depth of 100 m, the hydrostatic pressure is assumed equivalent to 1 MPa, thus critical buckling pressure must be greater than 1 MPa. The value obtained as shown in table 20 will then be called a measured value.

Table 20 Measured Value Total Deformation Load Multiplier

Measured Value	1.0575

5.2.2 Central Composite Diagram

In this report the Design of Experiment is generated using the Central Composite Diagram (CCD) method.

In Figure 43 below it can be seen that the DoE design point produces a set of data. The maximum and minimum load multiplier values and their comparison with measured value can be found in table 21.

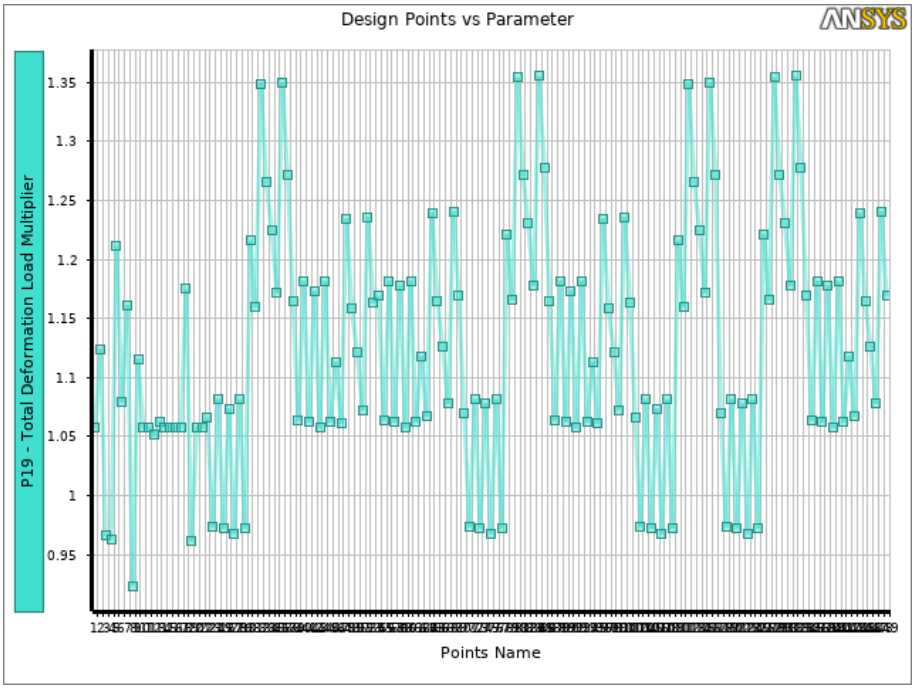

Figure 43 Design point vs Parameter, with Design of Experiment size N=149

Table 21 Comparison of the total deformation load multiplier from measured value with the Design of Experiment design point

Measured Value	Design of Experiment Central Composite Diagram	
	Minimum Value	Maximum Value
1.0575	0.9236	1.3553

It is interesting to note that the maximum value produced is significantly higher than the measured value. This difference is quite large, up to 28.16%. While the minimum value generated is smaller than the measured value with a decrease of 12.66%. Although the DoE Design Point provides the minimum and maximum values, the DoE has not been able to produce an optimal estimation value that can be used in the design.

The difference between the minimum and maximum values obtained from the DoE against the measured values indicates that a response surface methodology is needed to make the estimation values close to the measured value. The discussion regarding the response surface and optimization of the values obtained from the DoE design point will be discussed below.

5.2.3 Genetic Aggregation Response Surface

The DoE obtained in the previous step was further processed using the Genetic Aggregation Response Surface.

Table 22 Comparison of measured value, DoE value, and Genetic Aggregation value

Methodology		Value	% Error
Measured		1.0575	
DoE Design Point	Minimum	0.9236	-12.66
	Maximum	1.3353	28.16
Genetic Aggregation	Minimum	0.6475	-38.77
	Maximum	1.5331	44.97
	Estimated	1.0575	0

Table 22 shows a comparison between measured values, DoE values, and Genetic Aggregation values. It can be seen that the sample range used on the response surface is wider than the DoE range. This is understandable considering that the number of samples used in the response surface is much more than the DoE samples.

The highlight is that the estimated value given by the Genetic Aggregation response surface has zero percent error relative to the measured value. As already mentioned in sub-chapter 3.2.1 Genetic Aggregation response surface is a combination of other types of response surface. With an algorithm that allows to automatically selecting a response surface type that matches each parameter, the resulting estimate value is satisfactory.

The Goodness of Fit chart (Figure 44) generated by Genetic Aggregation response surface type shows that all of the estimated values generated by this response surface are perfect match with the reference value. The value for the average absolute error is 0.

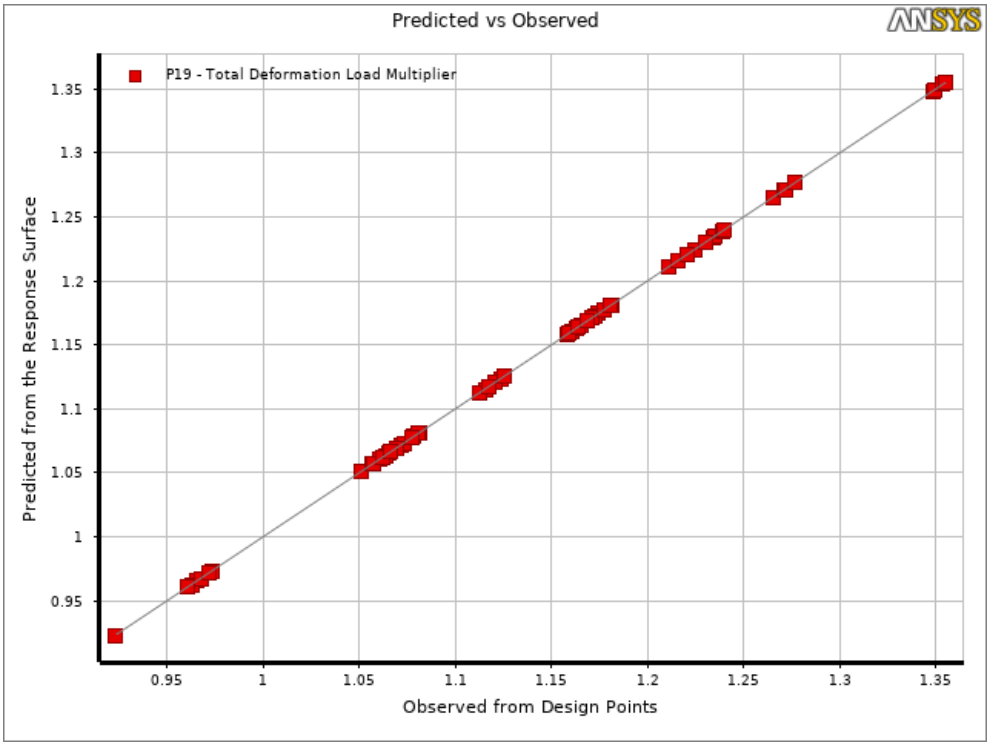

Figure 44 Genetic Aggregation Goodness of Fit for Total Deformation Load Multiplier

Figure 45 presents the response chart for the four main parameters that affect the pressure hull design. In Figure 45 a. the response chart shows the relationship between the cylindrical radius and load multiplier. This chart shows the relation between these two parameters has the same correlation characteristic as the correlation discussed in the parameter correlation study. This relation is negatively correlated. Cylindrical radius is inversely proportional to the load multiplier, thus the larger the cylinder radius, the smaller the load multiplier. As observed on the curve when cylindrical radius equal to 10566.67 mm. the response load multiplier is in the number 0.9989. In the radius below that number, the load multiplier is above 1.

Figure 45 b. explaining the relationship between web height and load multiplier is positively correlated. Observed on the curve, when the web height is equal to 592 mm, the load multiplier gives a response of 0.9924. This means that a pressure hull with a web height equal to or less than 592 mm will experience buckling.

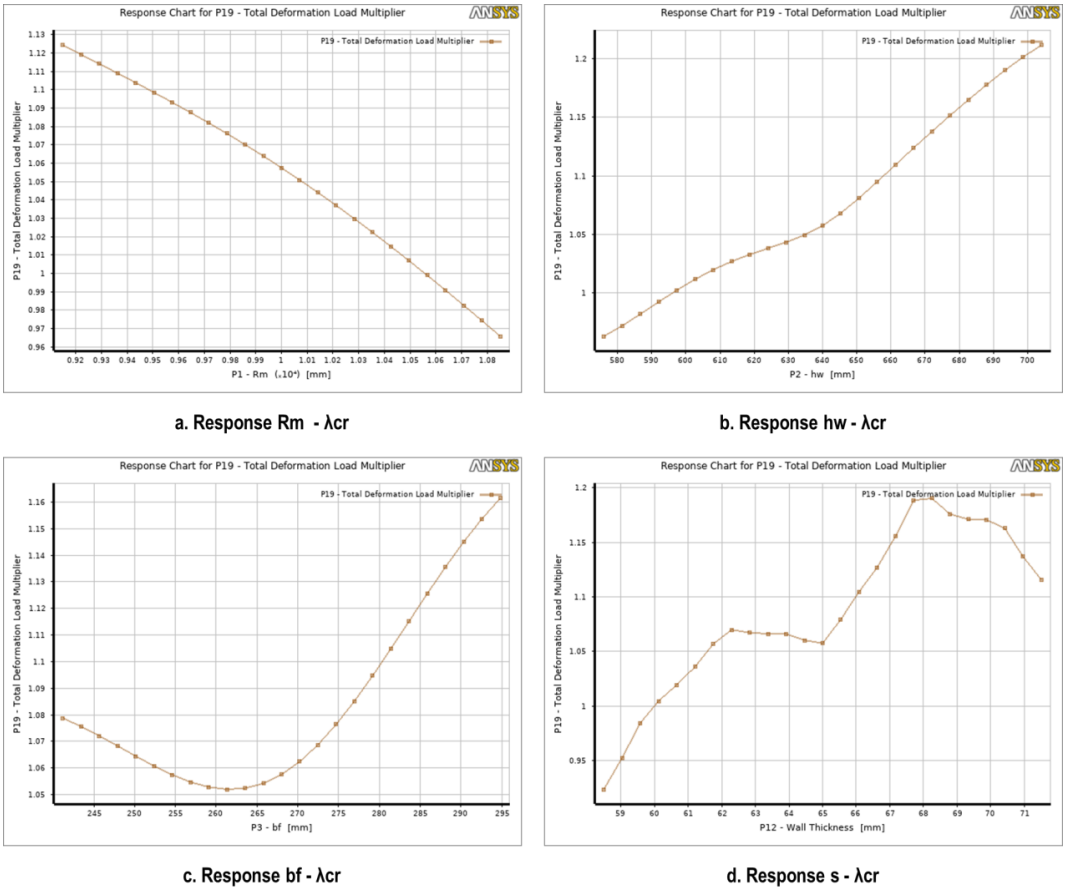

Figure 45 Genetic Aggregation response chart for the main four parameters

Interestingly, the relationship curve between the flange width and the load multiplier is shown in Figure 45 c. shows that the response point generated by the Genetic Aggregation type response surface has no flange width variation which causes the load multiplier value to be less than 1. In fact, the smallest response load multiplier number 1.0520 is generated when the flange width is 261.3 mm. Other flange width variation, within given range, either greater or less than 261.3 mm will result in a response load multiplier greater than 1.0520.

The final relation shown is the relation between the cylindrical wall thickness and the load multiplier. Although in general these two variables are positively correlated, there are several points where the relationship between the two is neutral. It can be observed on the curve when the cylindrical wall thickness is between 62 mm and 65 mm, the response load multiplier is almost the same.

5.2.4 Full 2nd Order Polynomial Response Surface

The DoE obtained in the previous step was further processed using the Full 2nd Order Polynomial Response Surface.

Table 23 Comparison of measured value, DoE value, and Full 2nd Order Polynomial value

Methodology		Value	% Error
Measured		1.0575	
DoE Design Point	Minimum	0.9236	-12.66
	Maximum	1.3353	28.16
Full 2nd Order Polynomial	Minimum	0.8154	-22.90
	Maximum	2.8556	170.03
	Estimated	1.0119	-4.31

It can be observed that this type of response surface provides a maximum value with an error of 170% and a minimum of -22.9% relative to the measured value. Even though the estimated value only misses -4.31%, this type of response surface cannot provide predictions that are close to the measured value. From a probability point of view, it can also be said that there is a possibility that this type of response surface will provide one extreme number that appears at a certain time frame. Hence, this type of response surface is not suitable to use.

The Goodness of Fit chart in Figure 46 reinforces the notion that this type of response surface is not accurate for analyzing a generated DoE dataset. It can be seen on the graph that many of the estimated values fall far from the line and some of them do not touch the line at all, which means this response surface unable to predict values for most of the DoE design points within its range.

Therefore, the Full 2nd Order Polynomial response surface type will not be discussed further.

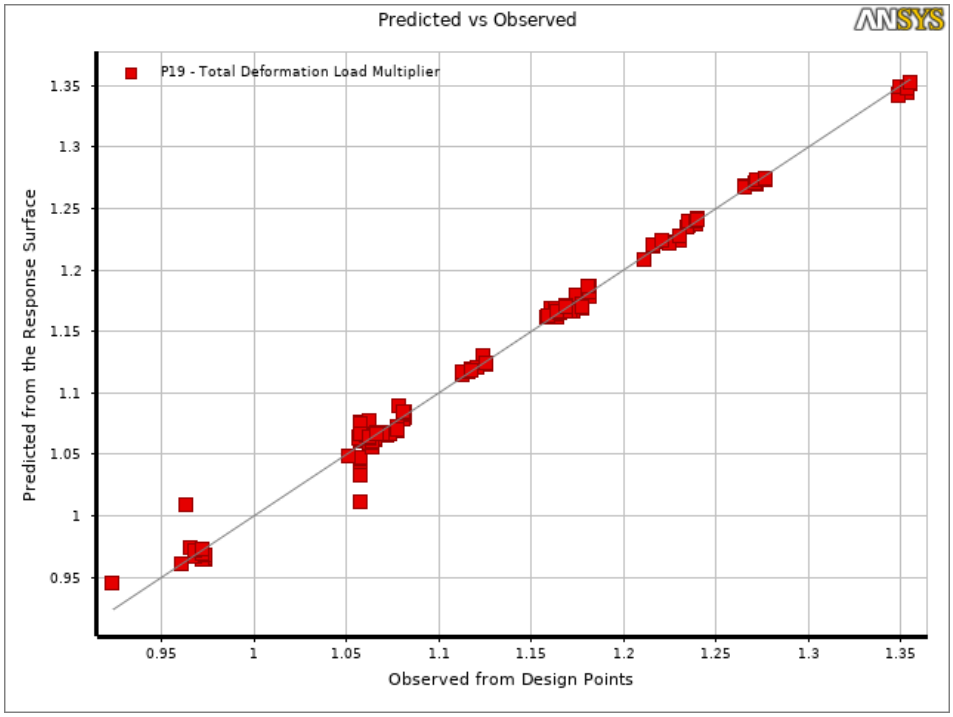

Figure 46 Full 2nd Order Polynomial Goodness of Fit for Total Deformation Load Multiplier

5.2.5 Kriging Response Surface

The DoE obtained in the previous step was further processed using the Kriging Response Surface.

Table 24 Comparison of measured value, DoE value, and Kriging value

Methodology		Value	% Error
Measured		1.0575	
DoE Design Point	Minimum	0.9236	-12.66
	Maximum	1.3353	28.16
Kriging	Minimum	0.3813	-63.95
	Maximum	1.6338	54.49
	Estimated	1.0119	-4.31

During the optimizing DoE using Kriging response surface, the maximum predictive error rate used is 5%. However, the refinement point in this experiment was not convergent and has an error of 5.9663%. Figure 48 shows un-convergence Kriging

response surface refinement point. This causes the level of accuracy of this response surface slightly fall for the desired predictive value.

However, shown in table 24 the estimated values generated by this type of response surface approximate the measured value. The Goodness of Fit chart in Figure 48 also shows the predictive value generated by the Kriging response surface which also falls right on the reference line. So it can be said that the Kriging response surface is able to predict the value for most of the given DoE design points.

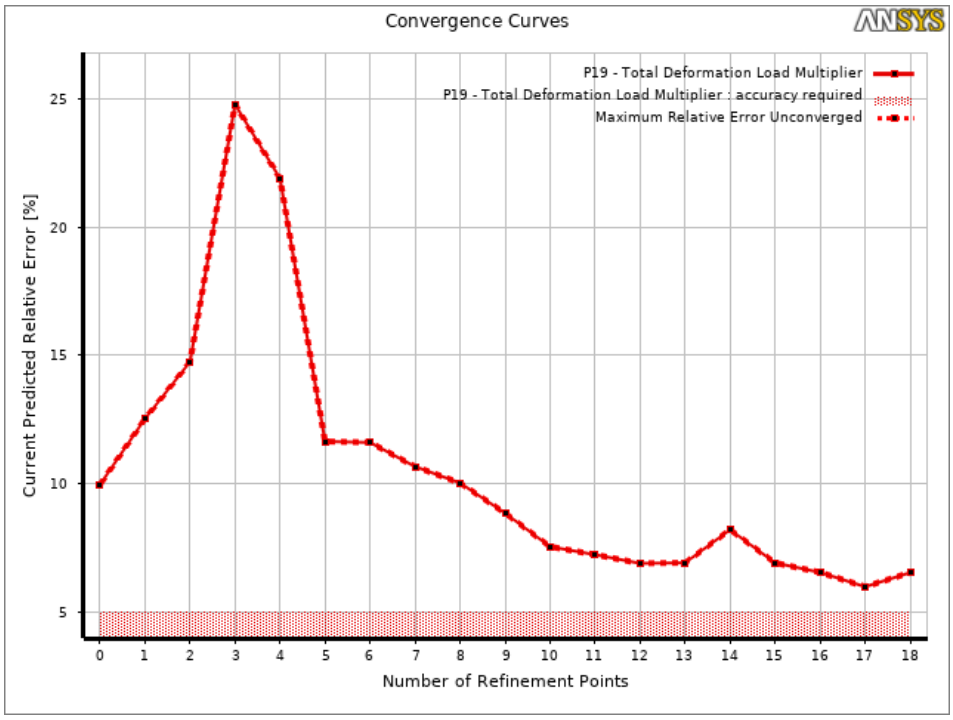

Figure 47 Un-convergence Refinement Points for max predictive error 5%

The relation between parameters for this type of response surface as shown in Figure 49 is also quite straightforward. Similar to the results of the interpretation in the correlation parameter study, the cylindrical radius negatively correlated with the load multiplier. Meanwhile, web height and cylindrical wall thickness have a positive correlation with the load multiplier. The relationship between flange width and load multiplier for Kriging respose surface has the same behavior as Genetic Aggregation response surface. Response surface Kriging does not predict load multiplier values below 1 for variations in flange width values within DoE range.

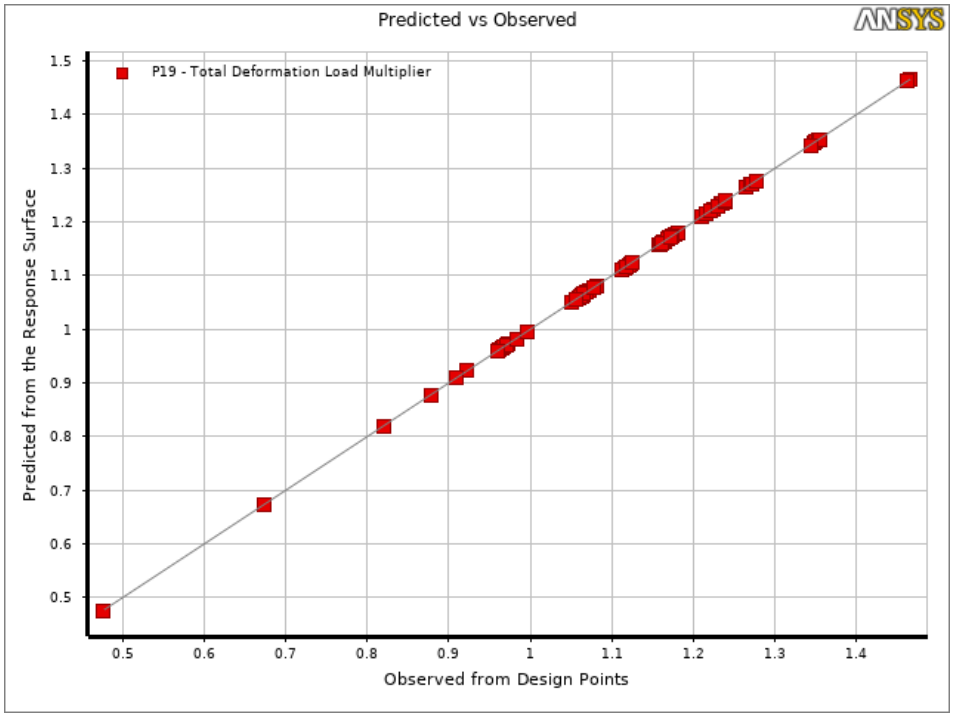

Figure 48 Kriging Goodness of Fit for Total Deformation Load Multiplier

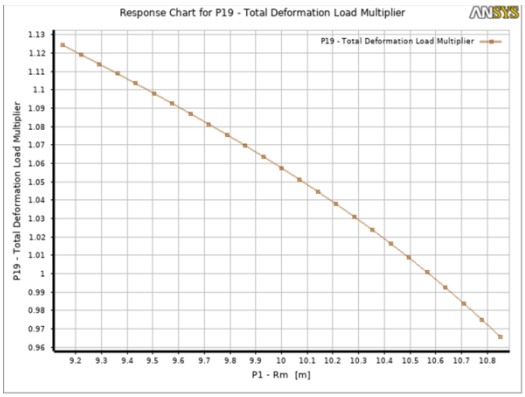

a. Response Rm - λcr

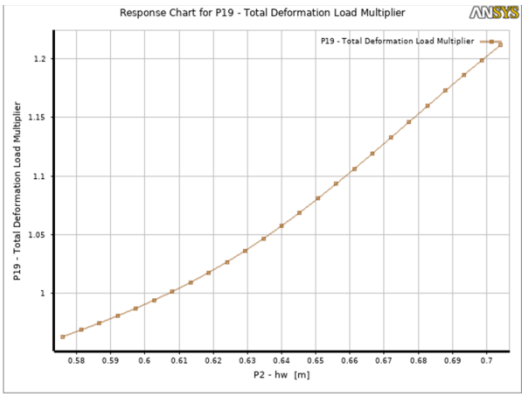

b. Response hw - λcr

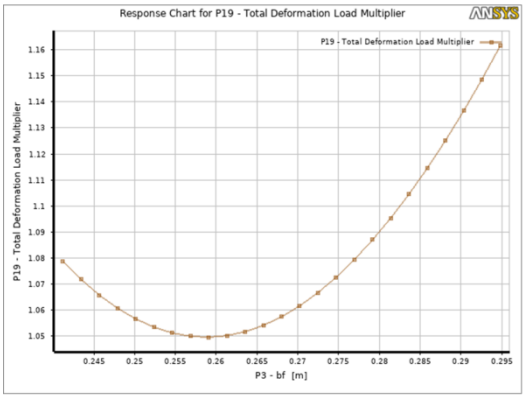

c. Response bf - λcr

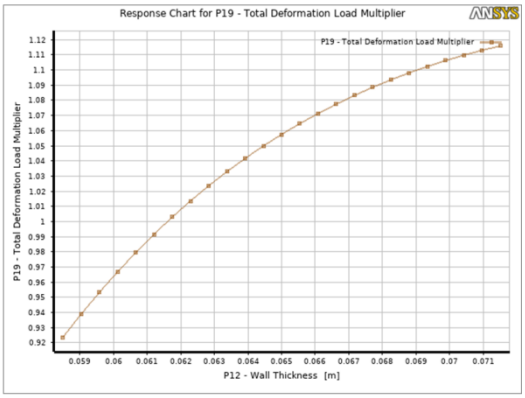

d. Response s - λcr

Figure 49 Kriging response chart for the main four parameters

5.2.6 Non-Parametric Regression Response Surface

The DoE obtained in the previous step was further processed using the Non-Parametric Regression Response Surface.

Table 25 Comparison of measured value, DoE value, and Non-Parametric Regression value

Methodology		Value	% Error
Measured		1.0575	
DoE Design Point	Minimum	0.9236	-12.66
	Maximum	1.3353	28.16
Non-Parametric Regression	Minimum	0.8128	-23.14
	Maximum	1.4596	38.02
	Estimated	1.0548	-0.26

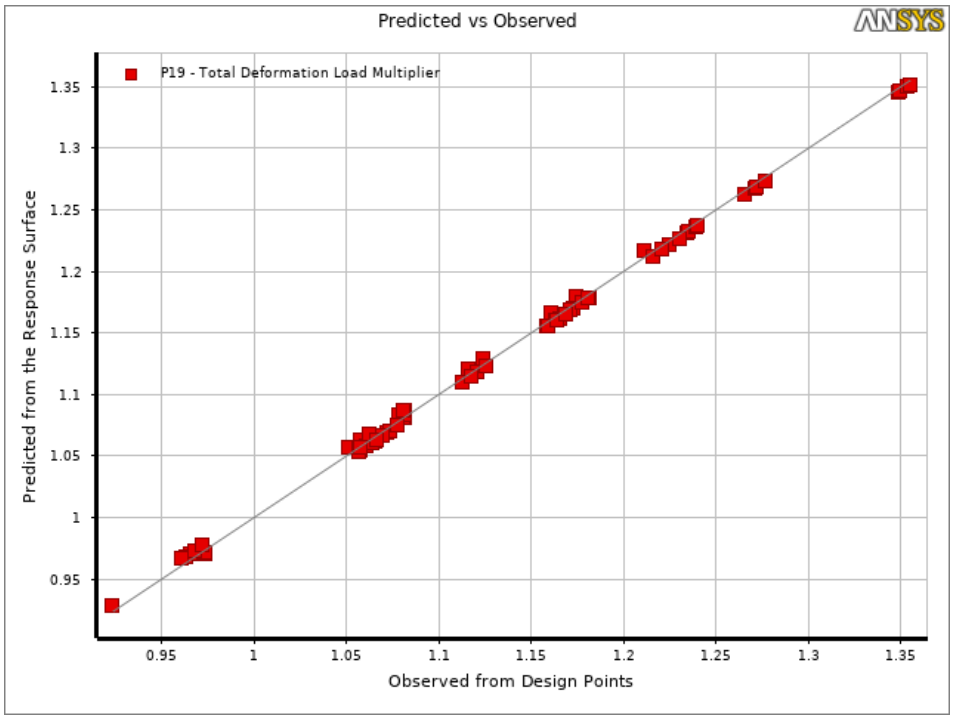

Figure 50 Non-Parametric Regression Goodness of Fit for Total Deformation Load Multiplier

Table 25 shows the comparison between measured value, DoE value, and the Non-Parametric Regression response surface value. The prediction value of the Non-Parametric Regression type response surface gives a result that is close to the measured value. The Goodness of Fit chart (figure 50) also indicates that Non-

Parametric Regression response surface is optimal for predicting the value of the DoE Design Point dataset. Considering the formula behind this response surface does not depend on given distribution or parameter, the predictive value is reasonable. The measured value was generated by taking into account the subsea shuttle is design to operate in 100 depths corresponds to 1 MPa or to load multiplier 1.0575. Therefore, this predictive value will indicate that the pressure hull will not reach the desired depth optimally.

5.2.7 Neural Network Response Surface

The DoE obtained in the previous step was further processed using the Neural Network Response Surface.

Table 26 Comparison of measured value, DoE value, and Neural Network value

Methodology		Value	% Error
Measured		1.0575	
DoE Design Point	Minimum	0.9236	-12.66
	Maximum	1.3353	28.16
Neural Network	Minimum	0.7785	-26.38
	Maximum	1.4965	41.52
	Estimated	1.0793	2.06

The estimated value generated by Neural Network has 2.06% relative to the measured value. This means Neural Network response surface predictive value unable to approach the measured value. Figure 51 Goodness of Fit for this response surface type also shows clustered predictive values which fall far from reference line. The average absolute error yields a big error of 23.278%. Therefore, it can safely assume the Neural Network response surface type is not suitable for the generated DoE Design Point data series.

The Neural Network response surface also will not be discussed further in this report.

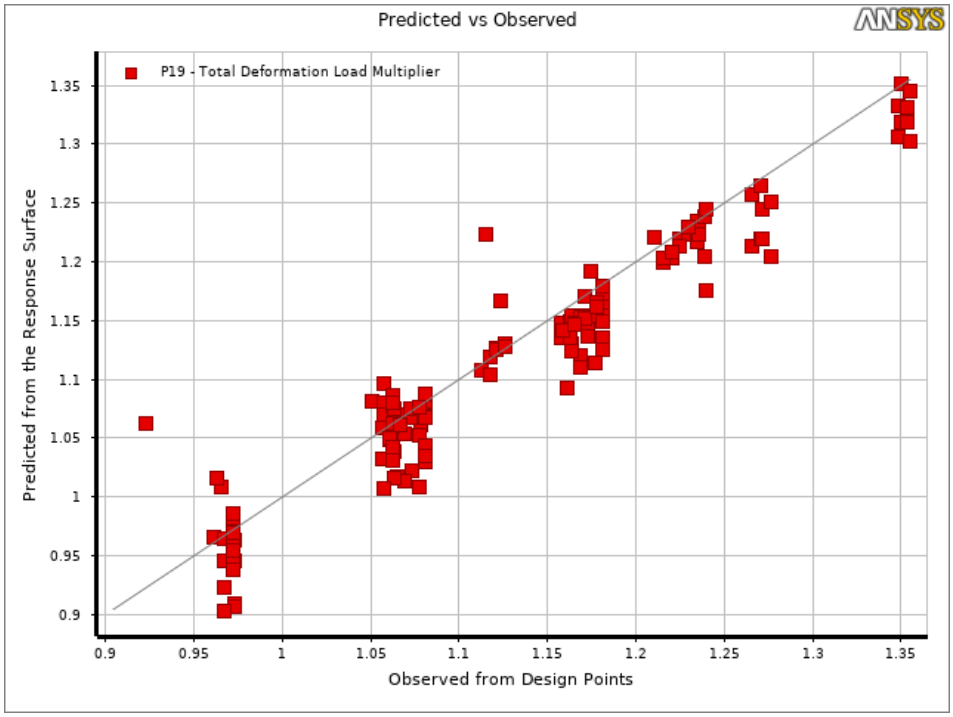

Figure 51 Neural Network Goodness of Fit for Total Deformation Load Multiplier

The following table is showing the resume all estimated value for different response surface type compared to the measured value.

Table 27 Comparison of measured value and response surface type value

Methodology		Value	% Error
Measured		1.0575	
Genetic Aggregation	Estimated	1.0575	0
Full 2nd Order Polynomial	Estimated	1.0119	-4.31
Kriging	Estimated	1.0575	0
Non Parametric Regression	Estimated	1.0548	-0.26
Neural Network	Estimated	1.0793	2.06

It can be observed that response surface type Genetic Aggregation and Kriging result are similar to the measured value. However, considering the un-convergence refinement point for the Kriging response surface, the Genetic Aggregation response surface provides the best result and will be selected for the Response Surface Optimization.

5.2.8 Response Surface Optimization

The response surface optimization is executed in order to obtain optimal results from a parameter by considering the existing objectives and constraints. Based on the results of the correlation parameter study, it can be observed that there are four main parameters that affect the ability of the pressure hull to withstand hydrostatic loads. However, of the four parameters, the cylindrical wall thickness has the highest correlation to the load multiplier compared to the other three.

In Chapter 1, one of the ways to optimize the weight of a pressure hull was discussed by making the component dimensions lighter. Therefore, to reduce weight without compromising the structural capability of the subsea shuttle pressure hull is to reduce the cylindrical wall thickness. Optimization of cylindrical wall thickness is the first objective and can be achieved by response surface optimization.

The subsea shuttle is expected to operate at a maximum depth of 100 m. The total deformation load multiplier that corresponds with this depth is 1.0575. In other words, the subsea shuttle pressure hull will fail if the hydrostatic load reaches 1.0575 Mpa. So it can be said that the subsea shuttle is only safe to operate at depth less than 100 m. The second target of the response surface optimization is to obtain the maximum load multiplier by optimizing the subsea pressure hull parameter dimensions. The domain setting for pressure is set so that the lower limit of this parameter is 1 MPa.

The objectives and constraints that have been established can be seen in table 28 below:

Table 28 Objectives and Constraint for Response Surface Optimization

Parameter	Symbol	Objective		Constraint		
		Type	Target	Type	Lower Bound	Upper Bound
Cylindrical Wall Thickness (in mm.)	s	Min	58.5			
Total Deformation Load Multiplier	λcr	Max	2	LB ≤ Value ≤ RB	1.0575	2

Table 29 presents the results of response surface optimization. ANSYS Workbench 2020 generates 3 candidate configurations according to the selected parameters. The displayed value also considers the objectives, constraints, and limits of each parameter.

Table 29 Response Surface Optimization Result

Parameter		Base	Candidate			Unit
			#1	#2	#3	
Cylindrical Mean Radius	Rm	10000	9209.67	9345.67	9182.47	mm
Web Height	hw	640	698.51	702.14	701.01	mm
Flange Width	bf	268	267.45	289.22	285.10	mm
Cylindrical Wall Thickness	s	65	58.73	58.90	60.89	mm
Bow Wall Thickness		65	59.68	61.84	67.56	mm
Aft Wall Thickness		65	70.76	62.95	67.63	mm
Web Thickness	sw	15	14.89	14.29	14.55	mm
Flange Thickness	sf	15	14.89	16.14	15.32	mm
Pressure	P	1	1.02	1.03	1.00	MPa
Force	F	2.0E+06	2.1E+06	2.0E+06	2.0E+06	N
Total Deformation Load Multiplier	λcr	1.0575	1.1404	1.1380	1.2233	
Critical Buckling Pressure	Pcr	1.0575	1.1673	1.1714	1.2240	MPa

Candidate #1

Based on the first objective of minimizing the cylinder wall thickness, the value for candidate #1 is very close to the target. 58.73 mm compared to the target value of 58.5 mm. Considering the second objective of maximizing the load multiplier, the value offered by this candidate is also larger than the base load multiplier. 1.1404 compared to 1.0575. Hence the critical buckling pressure went up from 1.0575 MPa to 1.1673 MPa. Overall candidate # 1 is able to optimize the basic parameters and able to satisfy the objectives.

Candidate #2

Candidate #2 is also able to answer objectives well. The value of cylindrical wall thickness in this configuration is 58.9 mm compared to the target value of 58.5 mm. Even though this value is larger than the value offered by candidate #1, when

compared to the base value of 65 mm, the value offered is acceptable. Furthermore, the candidate value for the load multiplier is 1.1380 compared to the base value of 1.0575. Thus, the critical buckling pressure increases from 1.0575 MPa to 1.1714 MPa.

Candidate #3

Candidate #3 offers a different configuration with the previous 2 candidates. Candidate values for cylindrical wall thickness of 60.89 mm were compared with target values of 58.5 mm. Compared to its competitors this value is in the last order. Although in general it is still decrease from the base value of 65 mm. However, the candidate score for the load multiplier increased considerably by 1.2233 compared to the base value of 1.0575. So the value of critical buckling pressure for this configuration increases from 1.0575 MPa to 1.2240 MPa. This means that the subsea shuttle with this configuration is capable of deeper diving than the other configurations. However, it needs to be considered, as stated by Burcher *et al* [6] that the deeper the level of the dive, the more supporting equipment needed.

In the ANSYS 2020 Workbench Response Surface Optimization tool, there is a trade-off feature that displays the comparison of the values of the three candidates. This feature provides 3 signs that represent the relationship between candidate values and objective values. Values that are considered close to the objective value will be marked with 1-3 stars. Candidate values far from the target value will be marked with 1-3 crosses. Meanwhile, candidate values that are close to the base value will be marked with a strip.

Based on this, the wall thickness optimization value for candidates #1 and #2 is given three stars and it can be interpreted that this value is very close to the target value. Meanwhile, the load multiplier value of the two candidates is given a strip. This means that it is considered still close to the base value. For candidate #3, the wall thickness cylinder value is marked with two stars, which means it is still close to the target value, but for the load multiplier value candidate #3 is marked with 1 star. By considering that the three candidate values are able to meet the specified target, it can be concluded that the response surface optimization process has succeeded in optimizing the base value.

6. Conclusion and Recommendation for Future Work

6.1 Conclusion

In this thesis report, the initial geometry of the subsea shuttle pressure hull is effectively prepared. The dimensions are arranged so that it is expected to be the first step in developing the subsea shuttle to answer the needs of alternative hydrocarbon transportation. The subsea shuttle pressure hull is modeled on a cylindrical shell configuration with a spherical domes and a fully conical shell at the other end.

A literature study was carried out to understand the physical phenomena and failure modes that may occur on the pressure hull subjected to external hydrostatic loads.

Finite element analysis modeling was executed to find parameters that significantly influence the pressure hull ability to withstand the external hydrostatic load. The results of the correlation study parameters found that there are four main parameters that affect the design. The four parameters are cylindrical shell radius, web height, flange width, and cylindrical wall thickness. Apart from these four parameters, frame spacing also affects pressure hull strength. This thesis report also compares numerical experiments based on DNVGL-RU-NAVAL Part 4 with the results of computational experiments to determine the characteristics and correlation between parameters.

Response surface methodology is used to further analyze the selected parameters. This report compares 5 types of response surface and it can be concluded that the Genetic Aggregation response surface gives the best results compared to other types. The best predictive value generated in the response surface study is optimized through response surface optimization. By determining specific objectives and constraints, response surface optimization succeeded in generating 3 best candidates which gave the optimal value of the desired parameters.

6.2 Recommendations for Future Work

Although submersible vehicles are widely available, the use of these vehicles as a means of transporting hydrocarbons is not yet available. The use of this vehicle as an alternative to hydrocarbon transportation requires different specifications from the military or recreational submarines. Hence, the subsea shuttle requires more intensive development. The following are recommendations that can be used to better develop the subsea shuttle.

- Define subsea shuttle Design Requirements and Objectives (DR&O) better. DR&O contains geometry, dimensions, utilization, and operation aspect. Hence, it will help determine the analysis direction and type in accordance with the development stage.
- The external load applied in this thesis is assumed to be uniform and evenly distributed on the outer shell of the pressure hull. In actual condition, this pressure is not uniform and uneven. Investigate how it affects the pressure hull shell.
- The thin shell is very prone to imperfection. The subsea shuttle pressure hull uses thin shell theory to analyze pressure hull shell strength. Investigate the existing imperfections for a better pressure hull design.
- The subsea shuttle is expected to be a vehicle that is able to go back and forth between oil and gas fields. Investigate dynamic load effect acting on the subsea shuttle.

7. Reference

[1] Whittle, T., *Fuelling the Wars - Pluto and the Secret Pipeline Network - 1936-2015*. UK: Folly Books Ltd. 2017.

[2] Morton, Q., *Beyond Sight of Land Oil: A History of Oil Exploration in the Gulf of Mexico*, vol. 30, issue 3. USA: GeoExpro. 2016.

[3] Chisholm, H., Ship in *Encyclopædia Britannica*. 24 (11th ed.) pp. 881–889. USA: A & C Black. 1991.

[4] Tolf, Robert W., *The Russian Rockefellers: The Saga of the Nobel Family and the Russian Oil Industry*. USA: Hoover Press. 1976. ISBN 0-8179-6581-5.

[5] Nash, William A., *Hydrostatically Loaded Structures: The Structural Mechanics, Analysis and Design of Powered Submersibles*, 1st edition. USA: Pergamon. 1995. ISBN 0-0803-7876-5

[6] Burcher, R, Rydill, L. *Concept in Submarine Design*, 1st edition. UK: Cambridge University Press. 1994

[7] Tafreshi, A. *Delamination buckling of composite cylindrical shells* in Delamination Behaviour of Composites. Cambridge-UK: Woodhead Publishing. 2008.

[8] Cook, Roberth D., Malkus, David S., *et al*. *Concepts and Applications of Finite Element Analysis*, 4th edition. New York-USA: Wiley, 2002.

[9] Bushnell, D., *Computerized buckling analysis of shells*. USA: Kluwer Academic Publisher. 1989.

[10] Pirie, W., Spearman Rank Correlation Coefficient in *Encyclopedia of Statistical Sciences*, 2nd edition. New Jersey-USA: John Wiley & Sons, Inc. 2006.

[11] Hinkle, D.E., Wiersma, W, Jurs, S.G., *Applied Statistics for the Behavioral Sciences*. 5th ed. Boston: Houghton Mifflin; 2003.

[12] Smith, M.J., Macadam, T., MacKay J.R,. *Integrated modelling, design and analysis of submarine structures. Ships and offshore structures*. 2015;10(4):349-66.

[13] Box, GEP., Wilson, KB., *On the experimental attainment of optimum conditions* (with discussion). J R Stat Soc Series B 1951; 13(1): 1-45.

[14] Calladine, C.R., Buckling of Shells: Classical Analysis, in *Theory of Shell Structure*, UK: Cambridge University Press, 1983, pp. 473–544.

[15] Reynolds, Thomas E., *Inelastic Lobar Buckling of Cylindrical Shells Under External Hydrostatic Pressure* DTMB_1960_1392

[16] DNV-RP-208 *Determination of Structural Capacity by Non-linear FE analysis Methods*, Norway. DNV. 2013

[17] DNVGL-RU-NAVAL Part 4 Chapter 1 *Sub-surface ships,* Norway: DNV. 2015

[18] Kavya, A., Prasanna, P., Jain, P.C., *Buckling Analysis of Ring Stiffened Circular Cylinders Using ANSYS*. International Journal for Research in Applied Science & Engineering Technology (IJRASET), 2017.

[19] Carlson, R. L., Sendelbeck, R. L., and Hoff, N. J., *Experimental Studies of the Buckling of Complete Spherical Shells, Experimental Mechanics*, Vol. 7, 1967, pp. 281-288.

[20] Hu, Y., Chen, B., and Sun, J., Tripping of Thin-walled Stiffeners in *the Axially Compressed Stiffened Panel with Lateral Pressure, Thin-Walled Struct.*, vol. 37, no. 1, pp. 1–26, May 2000, doi: 10.1016/S0263-8231(00)00010-0.

[21] Boresi, A.P., *Advanced mechanics of materials*. 6th ed. ed. Schmidt RJ, editor. New York: Wiley; 2003.

[22] Labovitz, S., *The assignment of numbers to rank order categories. American sociological review.* 1970, pp.515-524

[23] Ansys®. DesignXplorer. Release 2020 R2, help system, DesignXplorer User's Guide, Using Response Surfaces, ANSYS Inc.

[24] Pearson K. Notes on the history of correlation. *Biometrika*. 1920; 13(1): 25-45

[25] Jones, R.M., Buckling of Circular Cylindrical Shells, in *Buckling of Bars, Plates, and Shells*, Virginia: Bull Ridge Publishing, 2006, pp. 463–689.

[26] MacKay John R. *Structural Analysis and Design of Pressure Hulls - the State of the Art and Future Trends* in Technical Memorandum Defence R&D Canada. 2007

[27] Anderson-Cook, C., Douglas C. Montgomery, C., and Myers R., *Response Surface Methodology: Process and Product Optimization Using Designed Experiments*. 4th Edition. New York-USA: Wiley. 1995

[28] Montgomery, Douglas C., Guidelines for Designing Experiments in *Design and Analysis of Experiments*, 9th Edition, New York -USA: Wiley, 2017, pp. 17-19.

[29] Schneider, W. and Brede, A., *Consistent Equivalent Geometric Imperfections for the Numerical Buckling Strength Verification of Cylindrical Shells under Uniform External Pressure*. Elsevier. 2004.

[30] Zeman, JL., Rauscher, F., Schindler, S., General Term in *Pressure Vessel Design: The Direct Route*. Elsevier. 2006

[31] Donnell, LH., A New Theory for the Buckling of Thin Cylinder under Axial Compression and Bending, N.A.C.A Report No 473. 1934

[32] Friedman, N., *Submarine design and development*, Conway Maritime Press. 1984

[33] Granville, P.S., *Elements of the drag of underwater bodies*, DTNSRC-Report SPD-672-01

[34] Froude, W., *On experiments with HMS Greyhound*, Trans. Institution of Naval Architects 15, pp.36-73

[35] Ross Carl TF, *Pressure Vessels - External Pressure Technology.* Woodhead Publishing. 2011

[36] Gabler, U., *Submarine Construction*, DTNSRC-Report A059747

[37] Pohler, CH., Bement, AA., Wilson, AS., And Skinner, WA., *Submarine Main Ballast Tanks - Theory and Methods for Refined Structural Design*, DTNSRC-Report A0630820

[38] Lunchick, Myron E., *Plastic Axisymmetric Buckling of Ring-Stiffened Cylindrical Shells Fabricated from Strainhardening Materials and Subjected to External Hydrostatic Pressure*. DTMB_1961_1393

[39] Pulos, John C. und Salerno, Vito L., *Axisymmetric Elastic Deformations and Stresses in a Ring Stiffened, Perfectly Circular Cylindrical Shell under*

External Hydrostatic Pressure, DTMB_1961_1497

[40] Krenske, Martin A. and Kierman, Thomas J., *The Effect of Initial Imperfections on the Collapse Strength of Spherical Shells*, DTMB_1965_1757

[41] Blumenberg, William F., *The Effect of Intermediate Heavy Frames on the Elastic General-Instability Strength of Ring-Stiffened Cylinders Under External Hydrostatic Pressure,* DTMB_1965_1844

[42] Sharp, Arnold G., *Design Curves for Oceanographic Pressure-Resistant Housings,* TM WHOI-3-81

[43] Bagheri, M., Jafari, AA., and Sadeghifar, M., *Multi-objective optimization of ring stiffened cylindrical shells using a genetic algorithm*, J. Sound Vib., vol. 330, no. 3, pp. 374– 384, Jan. 2011, doi: 10.1016/j.jsv.2010.08.019.

[44] Ventsel, E. and Krauthammer, T., Survey of Elasticity Theory, in *Thin plates and shells: theory, analysis, and applications*, New York: Marcel Dekker, 2001.

[45] Chen, X. and Liu, Y., Finite Element Modeling and Simulation with ANSYS Workbench. CRC Press Tylor & Francis Group, 2015.

[46] Love, AEH., The Small Free Vibrations and Deformation of a Thin Elastic Shell, in *Philosophical Transactions of the Royal Society of London, Royal Society of London*, 1888, pp. 491–546.

[47] Balkin, SD., Lin, D., A neural network approach to response surface methodology, in *Communications in Statistics - Theory and Methods Journal*, vol. 29, pp. 2215 – 2227, 2000.

[48] [2015 ASME Section VIII division 2, *Boiler and Pressure Vessel Code*. American Society of Mechanical Engineers, New York, 2015.

[49] 2017 ASME Section VIII division 3, Boiler and Pressure Vessel Code. American Society of Mechanical Engineers, New York, 2017.

Appendix

Appendix A – Scatter Diagram

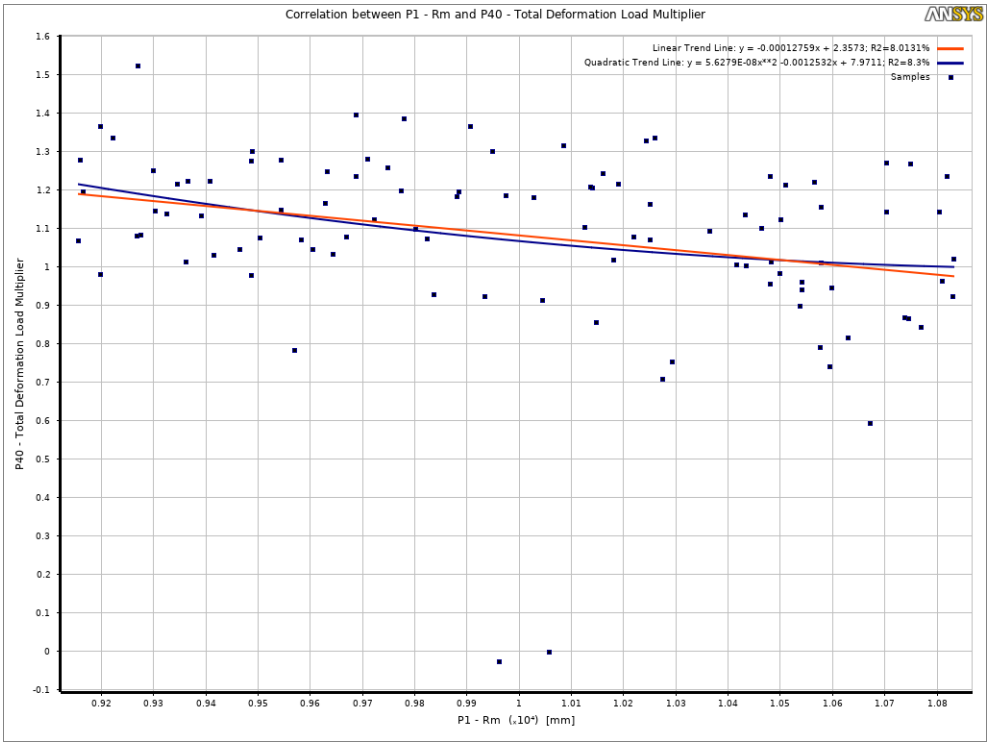

Figure 52 Scatter Diagram Cylinder Radius – Load Multiplier

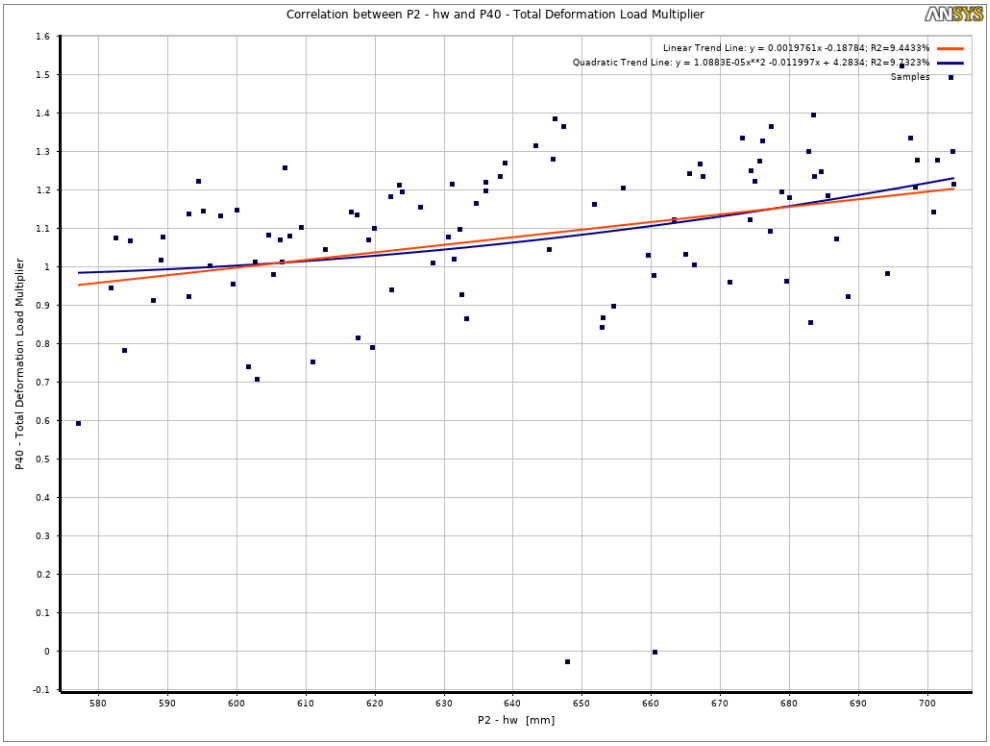

Figure 53 Scatter Diagram Web Height – Load Multiplier

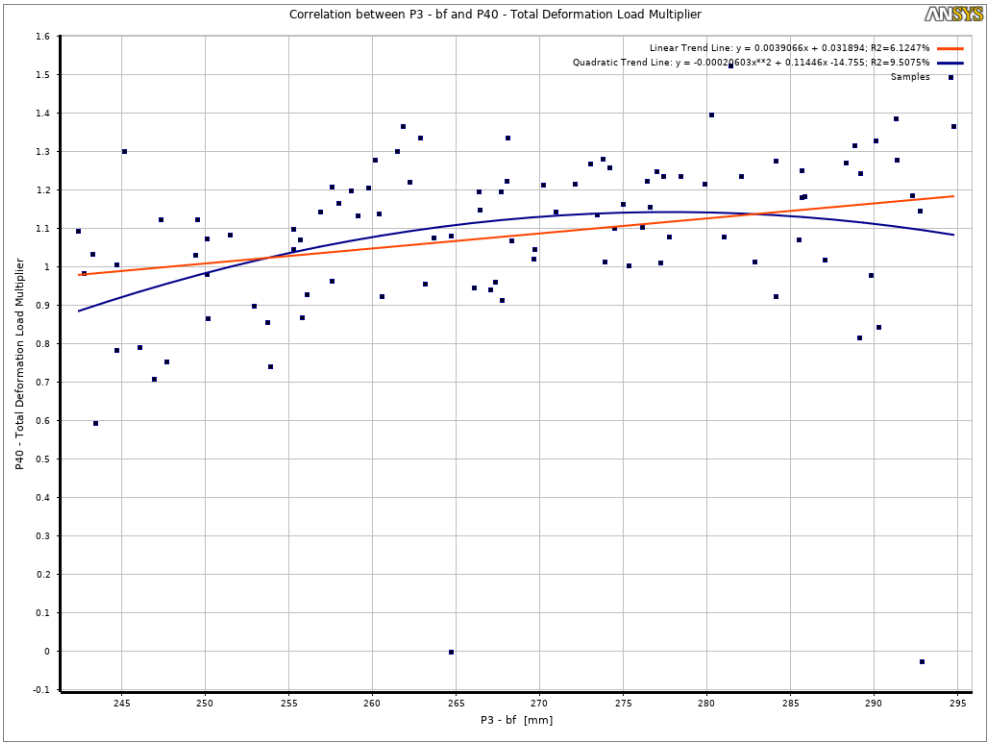

Figure 54 Scatter Diagram Flange Width – Load Multiplier

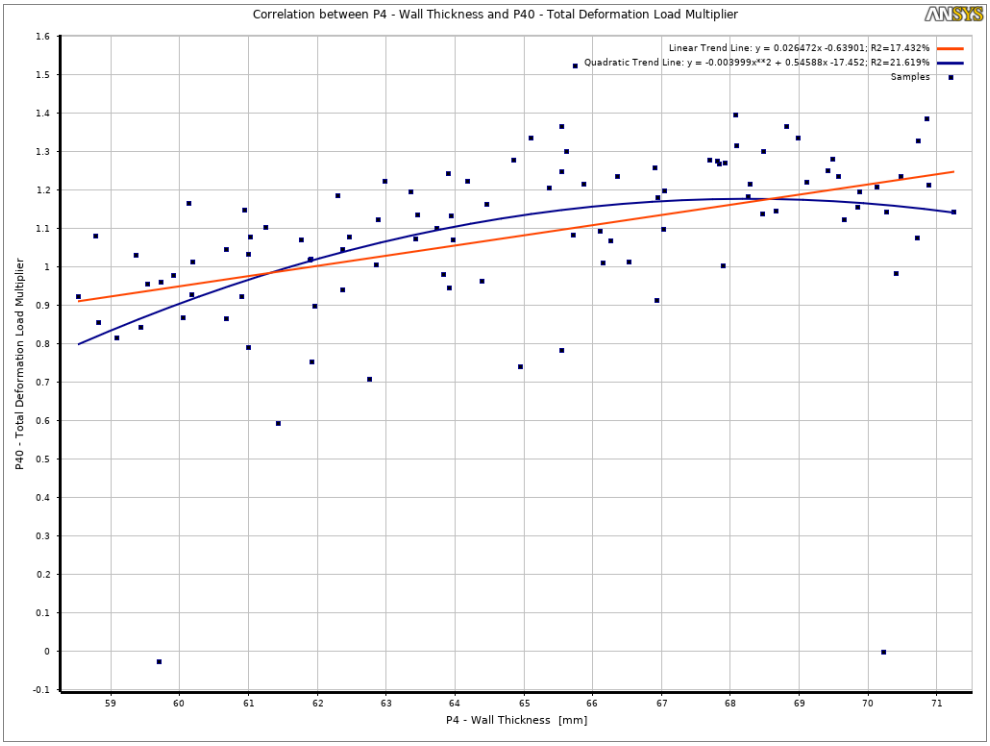

Figure 55 Scatter Diagram Cylinder Wall Thickness – Load Multiplier